Article

Direct comparison reveals algorithmic similarities in fly and mouse visual motion detection

Comparing algorithms for visual motion detection

starburst amacrine cell (SAC)

20 μm

vs.

T4,T5

Me
T4
T5 LoP
Lo
40 μm

Feature

Similarity

1. Uncorrelated and correlated noise

X R
Y T

++

2. Sinusoids and their sums

X R
Y T

1 s

+

3. Apparent motion

$(+,-, \rightarrow / \leftarrow)$

X R
Y T

250 μm

0 1 2 3 4

+/-

Juyue Chen,
Caitlin M. Gish,
James W. Fransen,
Emilio Salazar-
Gatzimas, Damon
A. Clark, Bart G.
Borghuis

damon.clark@yale.edu (D.A.C.)
bart.borghuis@louisville.edu
(B.G.B.)

Highlights

Calcium imaging compares motion processing in mouse and fly

Comparison finds strong similarities in responses to noise and correlations

Sinusoids elicit broad tuning in mice, with optima similar to flies

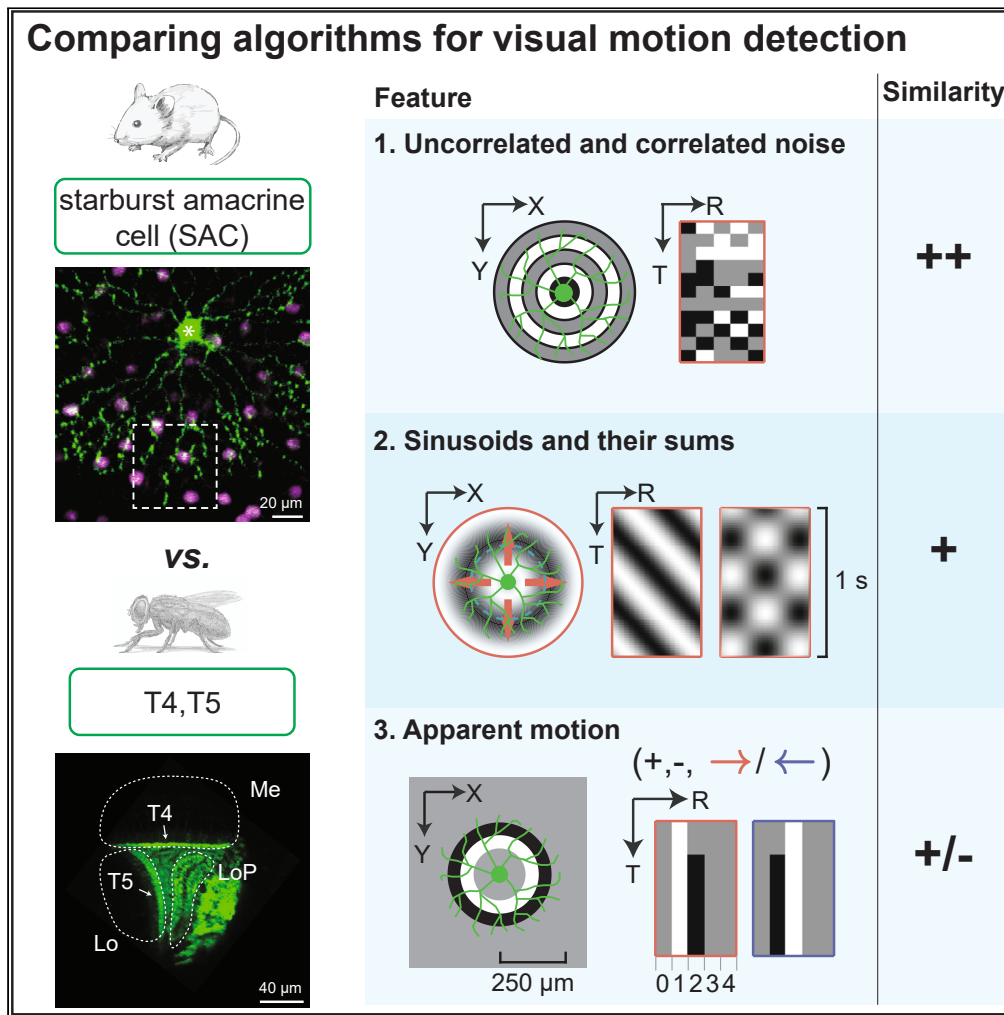Apparent motion stimuli elicit distinct response patterns in mice and flies

Article

Direct comparison reveals algorithmic similarities in fly and mouse visual motion detection

Juyue Chen,[1,6] Caitlin M. Gish,[2,6] James W. Fransen,[3] Emilio Salazar-Gatzimas,[1] Damon A. Clark,[1,2,4,5,7,*] and Bart G. Borghuis[3,7,8,*]

SUMMARY

Evolution has equipped vertebrates and invertebrates with neural circuits that selectively encode visual motion. While similarities in the computations performed by these circuits in mouse and fruit fly have been noted, direct experimental comparisons have been lacking. Because molecular mechanisms and neuronal morphology in the two species are distinct, we directly compared motion encoding in these two species at the algorithmic level, using matched stimuli and focusing on a pair of analogous neurons, the mouse ON starburst amacrine cell (ON SAC) and *Drosophila* T4 neurons. We find that the cells share similar spatiotemporal receptive field structures, sensitivity to spatiotemporal correlations, and tuning to sinusoidal drifting gratings, but differ in their responses to apparent motion stimuli. Both neuron types showed a response to summed sinusoids that deviates from models for motion processing in these cells, underscoring the similarities in their processing and identifying response features that remain to be explained.

INTRODUCTION

In both flies and mice, early visual circuits separately detect the movement of light and dark edges.[1] Strong parallels have been noted between the two systems in their anatomy,[2] circuitry,[3] and the suite of computations that they perform.[4] Because it is extremely unlikely that the visual systems of flies and mice derived from a common ancestor with any of those similarities in place, these parallels are interesting, as they may help expose constraints that limit the number and types of feasible solutions for motion detection. Yet, there have been no direct experimental comparisons between direction-selective cells in the two species that address this. One reason is that in these two widely diverged species, direction-selective cells have different morphologies and employ different neurotransmitters and receptors. Thus, the noted similarities between them necessarily exist not at the molecular level but at the *algorithmic* level.[5] The algorithm, for each species, describes mathematically how direction-selective cells respond to visual stimuli. This description is independent of low-level mechanisms and can be inferred from measurements of neuronal response properties. Mouse retinal physiologists and fly visual neuroscientists have traditions that use largely non-overlapping sets of visual stimuli, which have made direct comparisons between the systems difficult. In this study, we directly compared motion detection in the two visual systems by measuring calcium responses in mouse retina to a suite of informative visual stimuli and comparing them to the calcium responses of closely matched cells and stimuli in *Drosophila*.

In the mouse retina, the earliest direction-selective signals appear in starburst amacrine cells (SACs).[6] SACs comprise two classes, "ON" and "OFF'" driven by glutamatergic input from distinct bipolar cell populations activated by light increments and decrements, respectively[7,8] (Figure 1A). ON SACs respond selectively to moving ON-edges, while OFF SACs respond selectively to moving OFF-edges.[6,9] SACs have anatomically distinct, radially oriented neurites, each of which responds selectively to visual motion radiating away from the cell body.[6] SAC neurites appear to receive predominantly sustained bipolar cell input near the soma and predominantly transient input nearer to the release site at the dendritic tip.[10,11] These differential delays create an oriented filter in space and time,[9] which amplifies signals during radially outward motion and suppresses signals during motion in the opposite direction.[8] Several cellular and biophysical mechanisms have been shown to contribute to SAC direction selectivity,[12–17] but how they interact to generate the full direction-selective response remains incompletely understood.

[1]Interdepartmental Neurosciences Program, Yale University, New Haven, CT 06511, USA
[2]Department of Physics, Yale University, New Haven, CT 06511, USA
[3]Department of Anatomical Sciences and Neurobiology, University of Louisville, Louisville, KY 40202, USA
[4]Department of Molecular, Cellular, Developmental Biology, Yale University, New Haven, CT 06511, USA
[5]Department of Neuroscience, Yale University, New Haven, CT 06511, USA
[6]These author equally contributed
[7]These author equally contributed
[8]Lead contact
*Correspondence: damon.clark@yale.edu (D.A.C.), bart.borghuis@louisville.edu (B.G.B.)
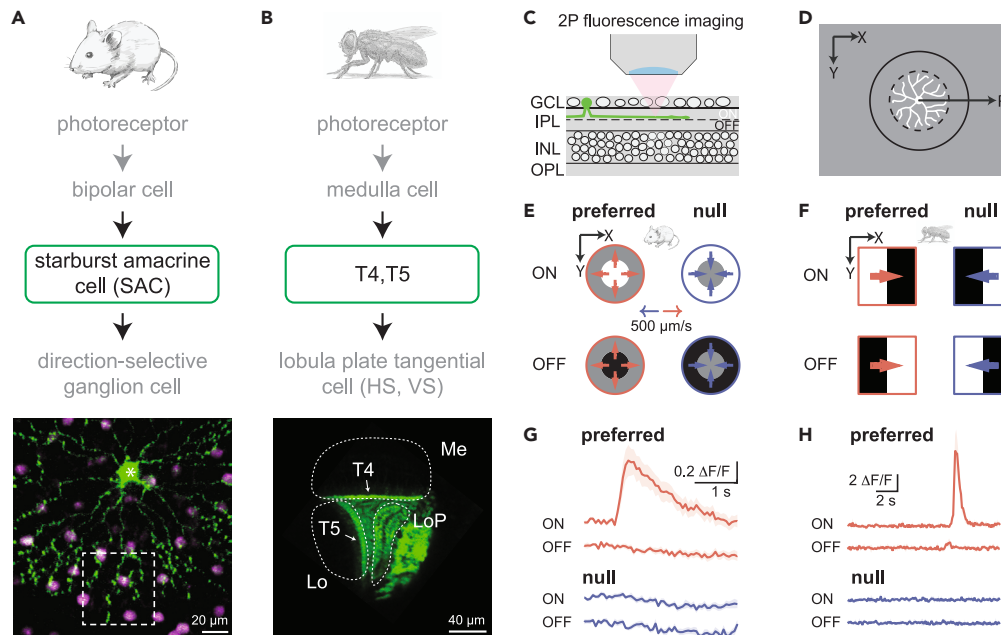https://doi.org/10.1016/j.isci.2023.107928

Figure 1. Elementary motion detectors in mice and flies are anatomically and morphologically distinct, but share similar responses to edge stimuli

(A) In mice, elementary motion detectors are starburst amacrine cells (SAC). Bottom: example two-photon fluorescence image of an OGB1-labeled SAC (green) surrounded by unlabeled SAC somas (magenta) in a ChAT-Cre x Ai9 mouse retina.

(B) In flies, elementary motion detectors are T4 and T5 cells. Bottom: 2-photon image of T4 and T5 cells expressing a fluorescent marker. Me: medulla; Lo: lobula; LoP: lobula plate.

(C) 2P fluorescence imaging of retinal explants was used to record visually evoked calcium responses in starburst amacrine cell neurites.

(D) Radially symmetric visual stimuli were centered on the soma of the recorded SAC (schematic morphology shown for scale; dashed line indicates the SAC dendritic field perimeter, solid line indicates stimulus perimeter). X and Y, x axis and y axis; R, radial axis.

(E) Bullseye edge stimuli used in SAC recordings. Dark and light edges moved in inward (null) or outward (preferred) directions.

(F) Edge stimuli used in T4 progressive cell recordings. Dark and light edges moved in a regressive (null) or progressive (preferred) direction across a background with opposite polarity.

(G) Average SAC distal neurite response to light and dark edges moving in the preferred (red) and the null (blue) direction. Shading represents ±1 SEM (n = 9).

(H) Responses of a sample T4 progressive region of interest, adapted from prior work.[18]

In the fly visual system, the earliest direction-selective signals appear in two identified neuron types, T4 and T5[19] (Figure 1B). These neurons respond to light and dark moving edges, respectively, similar to the ON-OFF split in mouse retina. The cell types are split into populations selective for the four cardinal directions, in contrast to the SAC dendrites, which respond to many different directions. T4 and T5 receive inputs from ON and OFF pathway neurons with delays that depend on their spatial position within the dendritic field.[20–25] The pattern of delays in each cell creates a spatiotemporally oriented linear receptive field.[26,27] This spatiotemporal organization of synaptic input resembles that of mouse ON and OFF starburst amacrine cells, as described previously. The inputs to T4 and T5 are integrated to generate mildly direction-selective membrane voltages and more direction-selective calcium signals.[28–32]

In this study, we gathered data on the response properties of mouse ON SACs to compare to the properties of T4 cells in flies. We compare the space-time receptive fields, responses to imposed correlations, responses to sinusoids, responses to summed sinusoids, and responses to apparent motion to test for algorithmic similarities in stimulus encoding. We found that across stimuli SAC calcium signals were less direction selective than T4 signals but that the tuning properties in most cases were quite similar. We found that T4 neurons and ON SACs show responses to summed sinusoids that are inconsistent with a broad class of linear-nonlinear models of direction selectivity and that the two cell types are notably different in their integration of ON and OFF visual signals in apparent motion stimuli.

RESULTS

To measure the algorithmic motion response properties of ON SACs, we used two-photon fluorescence (2P) calcium imaging in the whole-mount mouse retina. We measured visual stimulus-evoked calcium transients in the cells' distal dendritic varicosities, where they are presynaptic to both other SACs and downstream direction-selective retinal ganglion cells (Figure 1C). First, the cell-impermeant synthetic calcium dye Oregon Green 488 BAPTA-1 (OGB-1) was loaded into individual ON SACs by targeted electroporation (see STAR methods). We then presented visual stimuli using a bullseye paradigm, in which a radially symmetric luminance pattern on a photopic, mid-level gray background was centered on the soma of the recorded SAC (Figure 1D). The pattern extended out to a radius of 300 μm, well beyond the ~150 μm radius

of the SAC dendritic arbor and covering the antagonistic receptive field surround.[9,12,13] Because SACs are direction selective in the outward radial (centrifugal) direction, with individual dendritic segments acting as independent functional units,[6,33] this stimulus configuration permits experiments that activate all dendritic tips—the sites of synaptic output[8]—strongly and synchronously. The curvature in the bullseye stimuli is not typical of natural inputs to these cells, but by aligning with the directionality of the neurites, this stimulus drives the SAC maximally by providing the preferred stimulus throughout. This mimics comparable experiments in the fly, where stimuli were also aligned with cell directionality across the dendritic field.

We first measured calcium responses of the SAC to light (ON-) and dark (OFF-) edges moving in the preferred (outward) and null (inward) directions. As expected, and consistent with previous work,[6] ON SACs responded selectively to ON-edges in the preferred direction (PD) (Figures 1E and 1G). This same property exists in *Drosophila* T4 neurons (Figures 1F and 1H) and serves as the rationale for many parallels drawn between the two systems. Next, we proceeded beyond this elementary characterization and probed SAC response properties with a series of stimuli designed to determine the specific algorithmic similarities in processing in mouse SAC and fly T4 motion-signaling circuits.

Comparing calcium signals between cells

To compare algorithms in motion detectors in mice and in flies, it is important to determine first what comparisons are possible when one measures calcium using nonlinear, optical calcium indicators. Calcium signals could differ between cells when they have different baseline calcium concentrations or could appear different due to different nonlinearities and kinetics of the indicators. Our measurements in SACs were made using the small-molecule calcium indicator OGB-1, while the fly T4 measurements were made using the genetically encoded indicator GCaMP6f.[34] To gain intuition about how calcium signals will appear after being transformed by these two indicators, we created a simple dynamical simulation of each indicator and asked how each is expected to respond to a variety of different calcium traces (Figure 2, see STAR methods).

First, the two indicators have different binding constants, sensitivities to calcium concentration, and kinetics (Figure 2A). Differences in the binding constant have the potential to alter the apparent gain for different waveforms and basal calcium levels, as measured by $\Delta F/F$ (Figure 2B). Importantly, these apparent differences could occur even using a single indicator, for instance, if two cells have different basal calcium concentrations or between different indicators in the same or different cells (Figure 2B). Saturation of both indicators at high-calcium concentrations means that the indicator amplitudes need not be monotonic with calcium levels. As expected, the slower GCaMP6f indicator smears the computed responses more in time, so that for moderate frequency sinusoidal inputs, the indicator signal integrates calcium concentration over time, while OGB-1 does not. These results suggest that in making comparisons between cells or indicators, we should be wary of differences in amplitude or kinetics but can be confident that the sign of a change is a veridical representation of the true sign of changes in the calcium levels.

We next asked how systems identification approaches would be affected by different indicators and baseline calcium levels (Figure 2C and 2D). Here, we found that both indicators provided reasonable approximations of temporal filtering in calcium responses, with OGB able to better characterize filtering on fast timescales, due to its faster dynamics. As basal calcium levels increase, the timescales of GCaMP6f responses shorten, as expected from the binding equations (see STAR methods). When spatiotemporal filters were extracted (Figure 2E), the indicators smeared them in time, but the spatial structure remained true to the original filter. Thus, these results indicate that the spatial structure extracted from white noise presentation can be reliably compared between indicators, while the kinetic differences in indicators remain visible in the responses. Overall, our simulations show that one may compare calcium signals between different cells and indicators by focusing on features of the measured responses that are relatively invariant to changes in basal calcium and indicator. This largely means focusing on qualitative comparisons over quantitative ones, which we will do in this study.

Oriented space-time linear receptive fields

To characterize the visually evoked response properties of calcium in SAC dendrites, we presented uncorrelated binary noise in which each annulus of the bullseye pattern was updated independently every 33 ms to be white or black with 50% probability (Figure 3A). The central five of ten annuli covered the SAC dendritic field. During this stimulus presentation, we recorded calcium transients in the distal varicosities (Figure 3B).

We used a least-squares fitting procedure to determine the weighting of the stimulus, over time and space, that best predicted the measured calcium transients (Figure 3C). This weighting function is equivalent to the first-order Wiener kernel for the system[38,39] and can be visualized as a space-time plot. This weighting function has both positive and negative lobes, which represent positive and negative correlations between the stimulus luminance contrast and the measured calcium response, respectively. Consistent with the outward motion-tuned responses, the weighting function was oriented, or sloped, in space-time, which amplifies the response to stimuli moving in the outward, preferred direction, compared to the inward, non-preferred direction.[40]

The shape of the calcium kernel computed here is very similar to the shape of the voltage and current kernels measured previously in SACs.[9] The shape is also similar to kernels extracted from T4, using similar paradigms (Figure 3D)[26,27] and inferred from other experiments.[28] In both cases, a positive lobe weights stimuli in the receptive field center, while a negative one provides a delayed negative weighting in the receptive field periphery. We quantified the similarity in the shapes of the two receptive fields by computing the maximum cosine similarity between the functions, using different scalings in space and time, and shifting them spatially to find the maximum overlap (Figure 3E, see STAR methods). At roughly equal temporal scales and spatial scaling of ∼16 μm/°, the similarity score was ∼0.7, where similarity values could range from 1 (identical shape) to −1 (same shape, opposite signs). The SAC receptive field shape is consistent with the known anatomy and
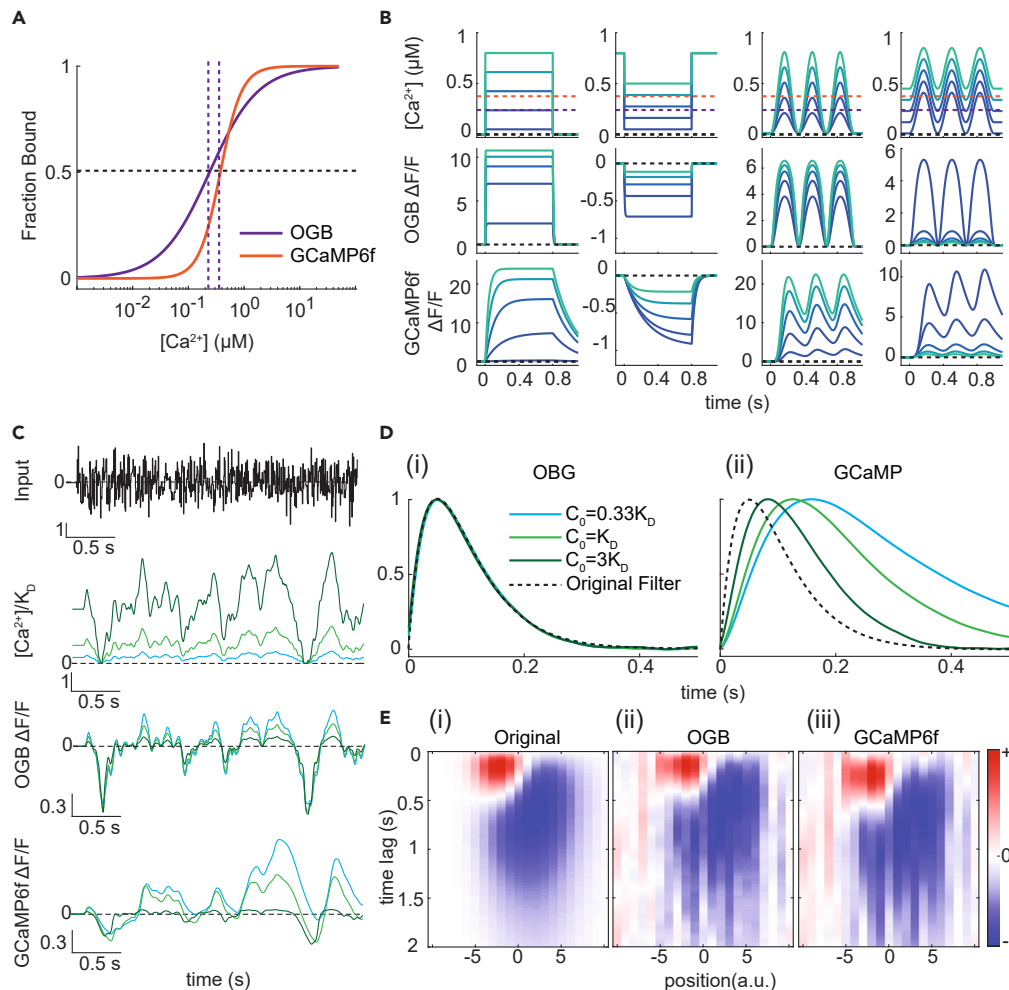
Figure 2. Different calcium indicators can capture qualitative similarities in response properties under different basal calcium conditions

(A) OGB1 and GCaMP6f have different steady state calcium binding curves, captured by a Hill function. The dissociation constant, K_D, defines the concentration of calcium at which one-half of indicator molecules are bound and is indicated by the vertical dashed lines. Parameters for the two calcium indicators are from[34–37] (see STAR methods).

(B) Simulated responses of OGB1 and GCaMP6f to step functions and sinusoidal functions of Ca2+ near the K_d of each indicator.

(C) Simulated responses of OGB1 and GCaMP6f to a Gaussian stimulus. A Gaussian random temporal stimulus (*top*) is passed through a temporal filter and given a range of basal calcium levels to generate distinct calcium traces (*second panel*). The simulated OGB (*third panel*) and GCaMP6f (*fourth panel*) responses are calculated from the calcium traces.

(D) Temporal filters were extracted using standard methods to obtain OGB1 and GCaMP6f filters of the stimulus under the three different calcium conditions in (C).

(E) Following the same procedure as in (C) and (D), a spatiotemporal filter (i) is used to model calcium responses to Gaussian spatiotemporal stimuli, which were used to compute receptive fields for the OGB1 (ii) and the GCaMP6f (iii) indicators.

physiology of the excitatory inputs,[8–10] while the negative lobe may be created by suppression of presynaptic bipolar cell excitation and direct inhibition from neighboring SACs.[12,14] In T4, the shape of the linear kernel is consistent with electrical measurements,[28] known anatomy of the circuit,[22] and the measured properties of upstream neurons.[21,24] In both SAC and T4 cells, the dynamics of the filter measurements are not much longer in duration than comparable electrical measurements, suggesting that the timescales measured here are not strongly influenced by indicator dynamics.

Responses to short timescale correlations

A linear kernel on its own is not sufficient to produce direction-selective average responses. This is because if stimuli are weighted linearly and averaged in time, a proximal stimulus followed by a distal stimulus yields the identical response as a distal stimulus followed by a proximal stimulus. Thus, a direction-selective average signal requires a nonlinear transformation of the stimulus,[40,41] making motion detection
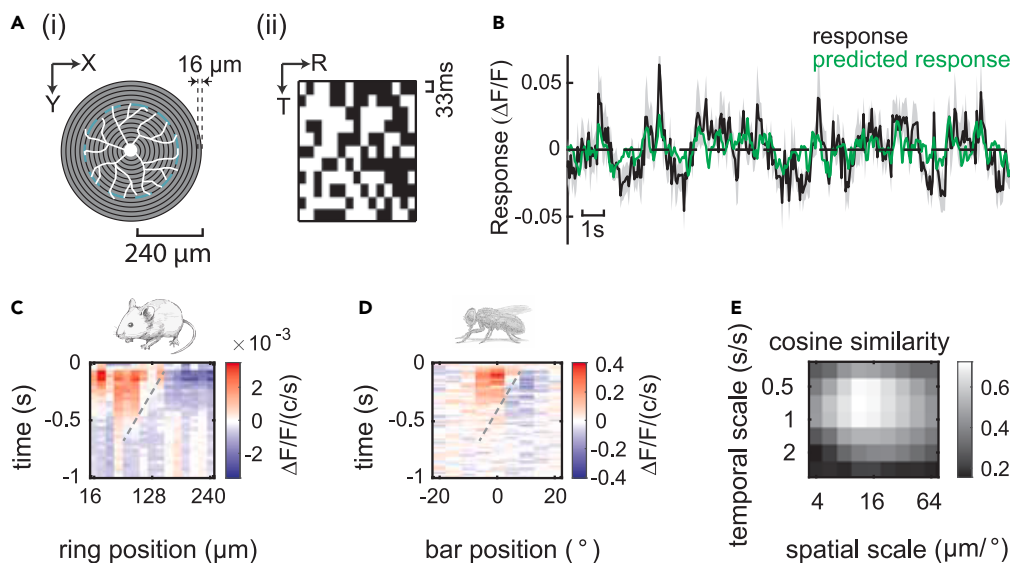
Figure 3. Comparison of linear receptive fields of SACs and T4 progressive cells

(A) Uncorrelated stochastic stimuli were presented to the mouse retina (i, bullseye stimulus; see STAR methods). (i) The stimulus for recording SACs comprised 15 concentric rings (ring width 17 μm; total stimulus diameter 510 μm) centered on the soma independent of neurite recording location and covered the receptive field center and surround. (ii) Space-time plot of an example fragment of the stimulus used in the recordings (R, radial distance; T, time).

(B) Averaged calcium responses (black) of SAC neurites evoked by the white-noise stimulus and predicted responses (green) based on convolution of the stimulus and linear receptive field. The linear filter acting on the stimulus predicted 50.3% of the variance in the measured calcium signal. Shading, ±1 SEM.

(C) Averaged SAC linear receptive field (n = 9) where x axis represents radial direction and y axis represents time in the past.

(D) Averaged linear receptive field of T4 cell in progressive layer.[27] The dotted line provides a guide to the eye; a more detailed analysis of the orientation of this receptive field is in the original study.[27]

(E) Similarity between mouse and fly scaled spatiotemporal receptive field computed using cosine metric. For each scaling, the similarity was computed at all displacements, and the maximum similarity is plotted.

fundamentally the detection of spatiotemporal correlations in the visual inputs.[42,43] We can characterize sensitivity to the simplest correlations by measuring the system's responses to pairwise spatiotemporal correlations in stochastic stimuli.[27,44,45] In the SAC, where voltages are predominantly linear transformations of the input,[9] the subsequent nonlinearity would likely stem from thresholding in voltage-gated calcium channels in the membrane.

To measure sensitivity to elementary (pairwise) spatiotemporal correlation, we created ternary stimuli that contained correlations between nearby pixels in space, at a variety of different offsets in time (Figure 4A). When this stimulus is presented to a neuron, the mean response during the presentation represents the neuron's sensitivity to that specific spatiotemporal correlation pattern, and the suite of responses to different temporal offsets can be thought of as the correlation-interval receptive field.[27] We updated the stimulus every 50 ms (three monitor frames) and measured calcium responses in SAC dendrites to 5 s presentations of these noisy stimuli (Figure 4B). We then assessed the direction selectivity of the response to each correlation interval by computing the mean response to centrifugal (preferred) displacement minus the mean response to centripetal (null) displacement (Figure 4C).

SACs were most responsive to correlations with ~50 ms lag, approximating the shortest stimulus update interval that reliably evoked tuned responses (see STAR methods). Responses dropped off quickly for lags of 100 ms and greater (Figure 4C). Interestingly, the SACs also responded to negative correlations, with ND orientations responding more strongly than PD orientations. These negative correlations correspond to "reverse-phi" motion illusions, which humans, mice, and flies all perceive.[27,46–50] The correlation interval responses in SACs look qualitatively similar to those in fly T4 neurons (Figure 4D), which also peak at fast times (~16–33 ms) and show inverted direction selectivity for negative correlations. While delays longer than the delay creating the largest response still elicited responses in flies, they elicited almost no responses in mouse. Importantly, the stimulus updates in the mouse experiments were designed to be slower than in fly experiments in order to elicit SAC responses, since vertebrate photoreceptor response dynamics are slower than those in insects.[51–53] In both mice and flies, the timescale of the peak correlation response is similar to the fastest timescales permitted by phototransduction.

Tuned responses to sinusoids

An alternative approach to assess sensitivity to different spatial and temporal scales evaluates responses to drifting sinusoidal gratings (Figure 5A). A drifting sinusoid is parameterized by its wavelength, λ, and its velocity, v. It has been useful to think of these instead as a spatial frequency equal to $1/\lambda$, and a temporal frequency equal to v/λ.[40] We presented drifting sinusoids and measured dendritic calcium signals for
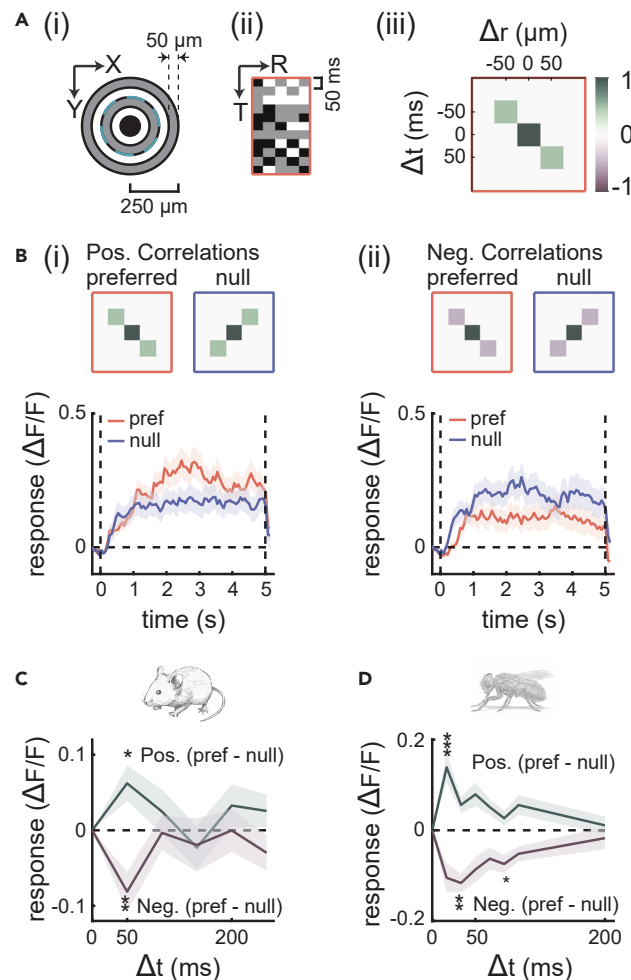
Figure 4. Responses to correlated stochastic stimuli in SACs and T4 progressive cells

(A) We presented correlated stochastic stimuli with positive and negative correlations, displaced in the preferred and null directions. The temporal offset was 50 ms. (i) An example stimulus frame (ring width 50 μm; total radial range 250 μm; dashed blue line indicates typical SAC dendritic arbor perimeter). (ii) Space-time plot of the visual stimulus (refresh rate 50 ms). R, radial axis in space; T, time. (iii) Auto-correlogram of the stimulus normalized by the correlation value at zero spatiotemporal offset.

(B) Average SAC neurite response (n = 54) to a stimulus with either a positive (i) or negative (ii) correlation in the preferred (red) or null (blue) direction. The correlation type is indicated in the auto-correlogram on top. Shading, ±1 SEM.

(C) Time-averaged direction selective (PD - ND) response of SACs to positive (green) and negative (purple) correlations (n = 54; *p < 0.05, **p < 0.01, ***p < 0.001 Wilcoxon signed-rank test, right-tail for positive correlation, left-tail for negative correlation. Bonferroni corrected for 10 comparisons). Shading, ±1 SEM.

(D) Time-averaged direction selective (PD - ND) response of T4 cells to positive (green) and negative (purple) correlations (positive, n = 23 flies; negative, n = 20 flies; *p < 0.05, **p < 0.01, ***p < 0.001, Wilcoxon signed-rank test, right-tail for positive correlation, left-tail for negative correlation. Bonferroni corrected for 14 comparisons). Shading, ±1 SEM. Data are adapted from previously published data.[27]

various spatial and temporal frequencies (Figure 5B). Both the sustained and phasic responses of the calcium signals depended on the spatial and temporal frequencies, as well as the direction of motion. To quantify this dependence, we computed the mean response to each spatial and temporal frequency pairing (Figure 5C). The SAC calcium signals were largest when sinusoids drifted in the preferred direction at frequencies of ∼3 Hz with a wavelength of ∼300 μm. Interestingly, this temporal frequency maximum is not so different from the maximum found in flies (Figure 5D), despite the differences in photoreceptor timescales as well as differences in the ecological motion signals the two animals are likely to detect. In both T4 and the SAC measurements, the tuning appears to be to stimulus temporal frequency (i.e., velocity divided by wavelength) rather than stimulus velocity,[54,55] though the broad tuning in the SAC makes this less pronounced. The tuning to temporal frequency is predicted by simple models of motion detection.[56] Although the GCaMP6f response measurements in flies could accumulate signal due to slow indicator dynamics (Figure 2), the effect on the measured tuning curves appears negligible.[27]

It is also interesting that the fly's spatial wavelength of maximum responses occurred at 30°-45°, around 2–3 times larger than the ∼15° span of inputs to the cell.[22] In the ON SAC, the responses were less peaked but were strong at 300 to 450 μm, also about 2–3 times the
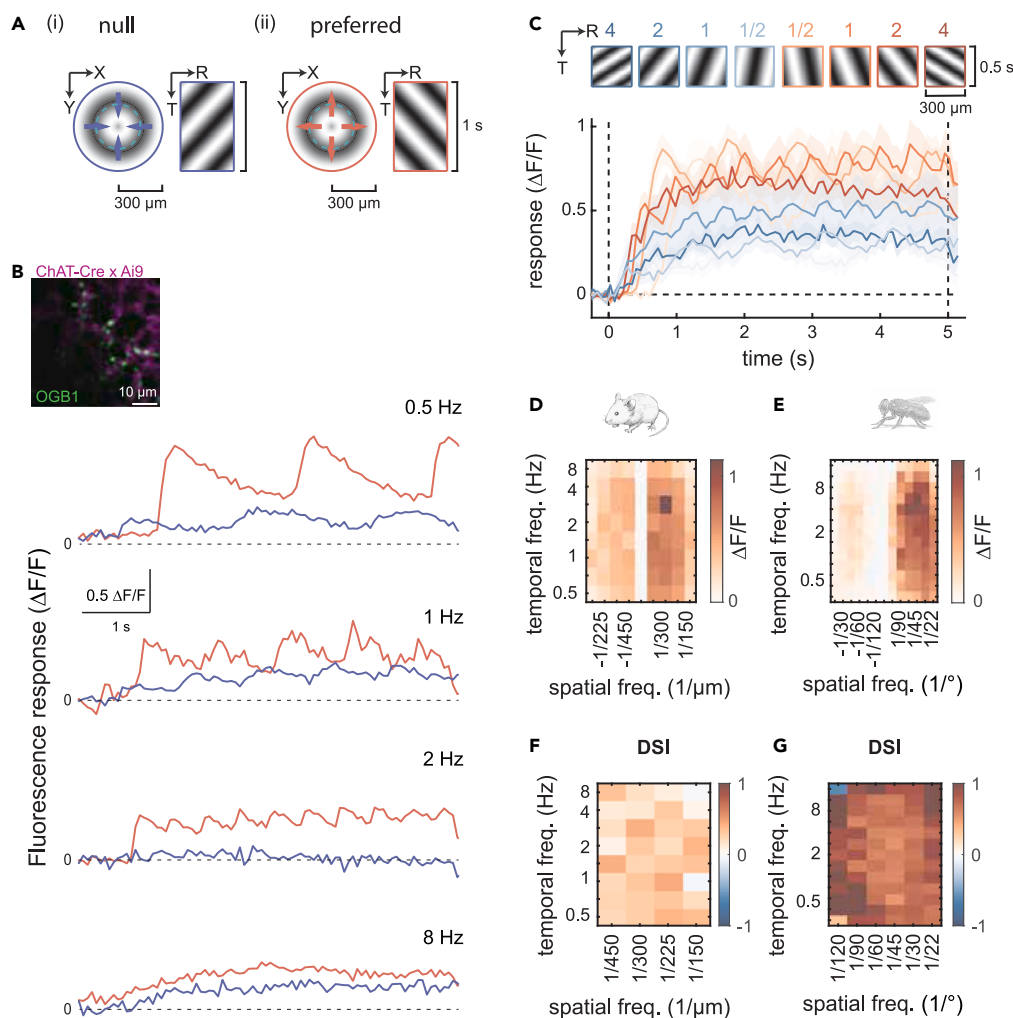
Figure 5. Calcium responses to sinusoidal stimuli show similar tuning in SACs and T4 cells

(A) Sinusoidal grating stimulus (see STAR methods) with a wavelength of 225 μm and a temporal frequency of 2 Hz moving in the null (i) and preferred (ii) direction. R, radial axis.

(B) Single trial OGB1 fluorescence responses of a SAC neurite during visual stimulation with sinusoidal gratings moving with various temporal frequencies. Wavelength 300 μm.

(C) Mean responses of SACs to sinusoidal gratings moving with various temporal frequencies, which are indicated in the space-time plot of the sinusoidal gratings on top. Wavelength 225 μm; shading, ±1 SEM (n = 22).

(D) Time-averaged (see STAR methods) response of SACs to sinusoidal gratings as a function of spatial and temporal frequency. Positive (negative) spatial frequency indicates the preferred (null) direction, or the outward (inward) direction. 100 μm across the mouse retina corresponds to ~3° of visual angle.

(E) Time-averaged response of T4 cells to sinusoidal gratings as a function of spatial and temporal frequency. Positive (negative) spatial frequency indicates the preferred (null) direction. Data are from prior measurements.[54]

(F and G) Direction-selective index (DSI) of SACs (F) and T4 progressive cells (G) at a range of spatial and temporal frequencies. DSI was defined as $\frac{r_{PD} - r_{ND}}{r_{PD} + r_{ND}}$, with r_{PD} and r_{ND} equal to the mean response over cells to PD and ND presentations.

~150 μm span of inputs to a single SAC dendritic branch. When there are only two inputs to a motion detector, there is a strong theoretical argument that the wavelength with maximum response should be 4 times the spacing between inputs,[57] or 2–3 times the receptive field size. With more complicated motion detection algorithms that receive more than two inputs, it is less clear whether there should exist a simple relationship between receptive field size and optimal wavelength.

Even though SACs and T4 neurons shared similar temporal frequency maxima, the measured calcium signals were notably different in their direction selectivity. SACs showed comparatively weak direction selectivity, responding to null direction stimuli only moderately less than preferred direction stimuli, consistent with recordings of SAC response properties and their postsynaptic direction-selective ganglion cell targets.[9,12,15,58–62] We quantified this using a direction-selective index (DSI), which divides the difference in preferred vs. null responses by their sum (Figures 5F and 5G). This index had a maximum value of ~0.2 for ON SACs with this stimulus, while in the fly T4 neurons, it was
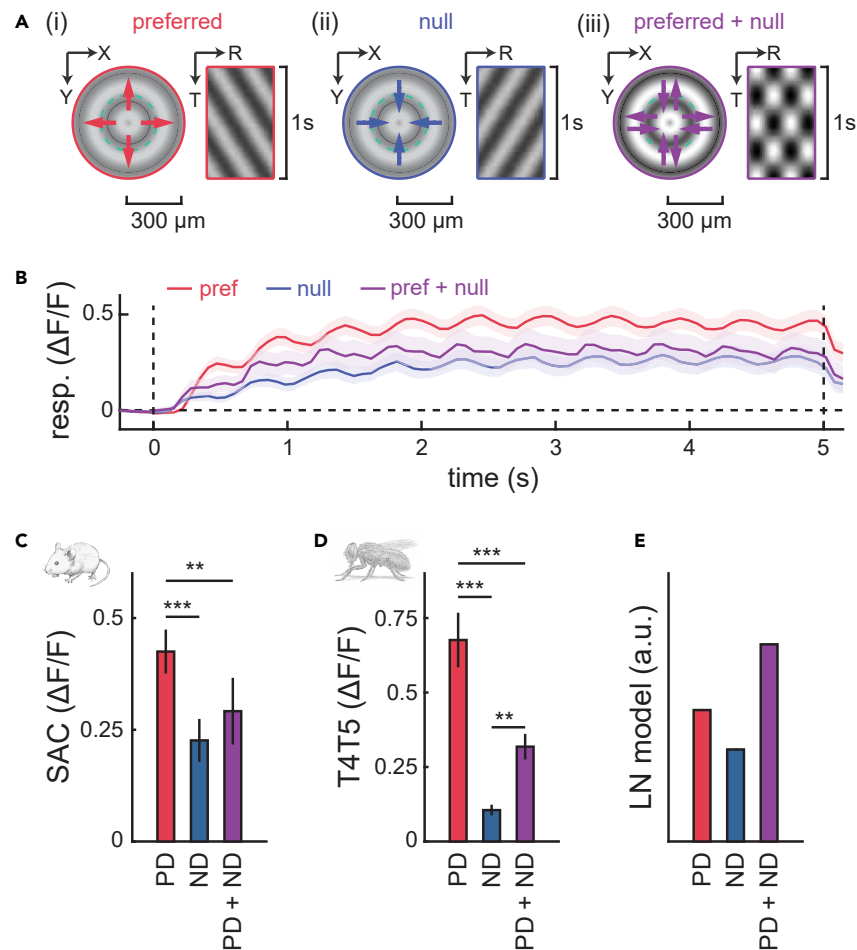
Figure 6. SAC and T4 cell responses show opponency

(A) Illustration of sinusoidal gratings drifting in the (i) preferred and (ii) null directions (wavelength 150 μm; temporal frequency 2 Hz). To avoid saturation of summed sinusoids, amplitude was 50% of maximum luminance contrast. (iii) When preferred and null direction sinusoids are added, the result is a 100% contrast counter-phase grating. Left panels show example frame (dashed line indicates SAC dendritic perimeter); right panels, space-time plots of stimuli.

(B) Average SAC response to sinusoidal gratings drifting in the preferred (red) and null direction (blue), and to counter-phasing sinusoidal gratings (purple). For all three curves, responses are averaged across 8 evenly spaced spatial phases. Shading, ±1 SEM (n = 23).

(C) Time-averaged responses of SACs in response to sinusoidal gratings and counter-phase gratings. Error bar, ±1 SEM (n = 23, *p < 0.05, **p < 0.01, ***p < 0.001 Wilcoxon signed-rank test, right-tail for response to preferred direction over counter-phase gratings, two-tailed for the rest; Bonferroni corrected, m = 3).

(D) Time-averaged responses of T4 cells in response to sinusoidal gratings and counter-phase gratings. Error bar, ±1 SEM (n = 17 flies, *p < 0.05, **p < 0.01, ***p < 0.001, Wilcoxon signed-rank test, right-tail for response to preferred direction over counter-phase gratings, two-tailed for the rest; Bonferroni corrected, m = 3). Fly data are adapted from a prior study.[30]

(E) Schematic responses of a linear-nonlinear (LN) model to sinusoidal gratings and counter-phase gratings. When the nonlinearity is convex, then for any linear filter the counter-phase gratings generate a larger response than the preferred direction sinusoid.[30]

around 0.8 or above for a wide range of stimulus parameters. We discuss later how to interpret this result in light of the different calcium indicators and nonlinear signal transduction steps in these cells.

Opponent responses to sinusoids

A simple, informative approach to studying algorithmic properties of neurons is to ask how they respond to sums of sinusoidal gratings. In one spatial dimension, the simplest version of this is to compare responses to preferred and null direction gratings to responses to stimuli composed of the sum of preferred and null direction gratings (Figure 6A). The sum of two sinusoidal gratings with opposite velocities is a counterphase grating, which appears visually stationary and has twice the contrast of the two-component sinusoids (see STAR methods). Comparisons of responses to such stimuli have been used to evaluate the linearity of cellular responses[29,63] and have also been used to test models for direction selectivity.[30,64]
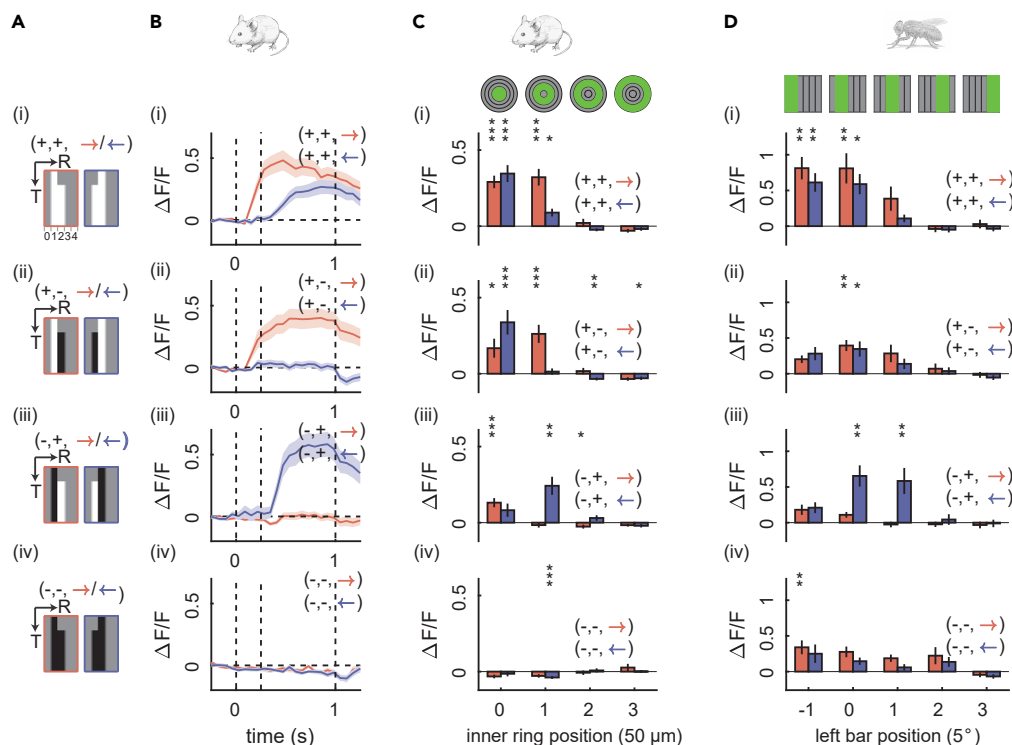
Figure 7. Responses of SACs and T4s in response to apparent motion stimuli

(A) Space-time plot of eight apparent motion stimuli (two per subplot; see STAR methods) at position with index of 1 and 2. The contrasts of leading ring and lagging ring in the apparent motion have four possible combinations: light-light (i), light-dark (ii), dark-light (iii), and dark-dark (iv). If the inner bar appeared 250 ms before the outer bar, the stimulus displacement is in the preferred direction (red). The null direction (blue) is the opposite.

(B) Responses of SACs to apparent motion stimuli shown in A. Three vertical dashed lines indicate the onset of the leading ring, the onset of the lagging ring, and the offset of both rings. Shading, ±1 SEM (n = 28).

(C and D) Time-averaged responses of SACs (C) and T4 progressive cells (D) to apparent motion stimuli at various spatial locations, illustrated in green on top (*p <0.05, **p <0.01, ***p <0.001, Wilcoxon signed-rank two-tail test, Bonferroni corrected by number of comparisons, m = 10, 16 for SACs and T4 progressive cells, respectively.) Fly data are adapted from prior work.[49] Error bars, ±1 SEM.

We found that in ON SAC dendrites, calcium signals in response to counterphase gratings had an amplitude that depended on the spatial phase of the counterphase grating (Figure 6B). When averaged over these spatial phases, responses to the counterphase grating were in between responses to the preferred and null components alone (Figure 6B). Thus, the mean response to the counterphase grating is less than the PD component alone, even though contrast is twice as large for the counterphase grating in these experiments (Figure 6C). Interestingly, this pattern of responses matches closely responses found in T4 and T5 cells in flies (Figure 6D).[30]

In these experiments, one may think of the counterphase response as the response when null direction sinusoids are added to the preferred direction stimulus. For both the SAC and T4, this *lowers* the response. Thus, this response property can be considered a general form of direction opponency, in which null direction motion decreases the response of the cell.[30] Importantly, this response property cannot be generated by linear-nonlinear models with an expansive nonlinear step (Figure 6E).[30,65] While this sort of simple linear-nonlinear model has been used frequently to explain responses in direction-selective cells,[9,26,29,40,66,67] the response property observed here, in fact, excludes such models for ON SACs. Alternative models, including those that incorporate realistic input rectification, synaptic conductance, or dynamic nonlinearities may instead explain these results.[28,30,65,68] Importantly, SAC neurites receive inhibitory synaptic input with opposite directional tuning from neighboring SACs and non-SAC amacrine cells,[12,13] which could also drive the observed opponency in SACs.

Responses to apparent motion

Last, we asked how SACs respond to apparent motion stimuli, in which nearby points in space are sequentially lightened or darkened (Figure 7A). We designed a stimulus that allowed a total of eight light-dark-direction combinations presented at a variety of eccentricities relative to the SAC center. We measured calcium responses to each stimulus combination at each of the four spatial positions relative to the SAC neurite (Figure 7B). This spacing of the pixels was selected to approximate the spatial scale of the bipolar cell receptive fields that underlie the excitatory inputs to the SACs.[9]

The ON SAC responded to stimuli containing contrast increments primarily when these were presented over the neurite. These responses are consistent with the measured linear receptive field (Figure 3), and also with prior experiments that used a light-light apparent motion

stimulus.[12] The strongest responses were evoked by outward light-light apparent motion, by outward light-dark, and by inward dark-light (Figure 7C). Dark-dark apparent motion evoked virtually no responses. The calcium signals appear driven primarily by responses to the individual bars at each point in space (Figure S1). The inward light-light pairing was weaker than the inward dark-light pairing (Figures 7Bi and iii), likely because the light-light pairing activated a neighboring SAC that inhibited the measured SAC. These SAC responses differ from those found in T4 cells, which respond strongly to the light-light pairing in the preferred direction[69] and to the dark-light pairing in the null direction but not strongly to light-dark pairings in the preferred direction (Figure 7D).[49] The absence of strong direction selectivity to the negative correlations in the apparent motion stimuli is in contrast to the response inversion in the correlated noise stimulus (Figure 4); the strength of the apparent motion stimulus could recruit a different set of nonlinear properties from the relatively weak but highly directional correlated noise stimuli. In contrast to the SAC, in the fly eye, the pairing of preferred direction, same-contrast responses with null direction contrast-inverting responses appears to underlie behavioral responses to apparent motion and especially to "reverse-phi" apparent motion.[49]

DISCUSSION

In this study, we investigated the algorithmic similarity between two identified direction selective neuron types in the visual systems of mouse and fly, ON SACs and T4 neurons. We found four specific similarities between the cells' motion-evoked responses. First, the linear weighting function of calcium responses in ON SACs and T4 cells share similar oriented space-time structures, as expected (Figure 3). Second, responses to spatiotemporal correlations were tuned to relatively fast timescales in both cells and sensitive to both positive and negative correlations (Figure 4). Third, the two cells show similar tuning to sinusoids of varying spatial and temporal frequencies, though the T4 cell calcium signals were more direction selective than those in ON SACs (Figure 5). Fourth, both ON SACs and T4 cells responded to summed opposite-direction sinusoidal stimuli in a way that cannot be accounted for by a linear-nonlinear cascade model with a typical, expansive nonlinearity (Figure 6). The mechanistic basis for these responses in SACs is of interest and for now, remains unclear. We also report one categorical difference between ON SACs and T4 cells, which pertains to the response to apparent motion stimuli of opposite contrast polarity. The measured responses in T4 cells bear the signature of the known "reverse phi" motion percept, whereas SACs for stimuli of the same contrast polarity show the expected direction-tuned response, and for contrast reversing stimuli appear to be driven primarily by the local light or dark contrasts rather than their sequential appearance (Figure 7).

Models for SAC direction selectivity

The voltage signals in SACs approximate linear transformations of visual stimuli,[9] but the calcium signals measured here and elsewhere are direction selective.[6] These observations have led to linear-nonlinear (LN) models to explain SAC direction selectivity.[9] In these models, the membrane potential is a linear transformation of the stimulus, and a static nonlinearity—often a threshold-linear transformation—is applied to the linearly filtered stimulus to generate a directional signal. Such models are closely related to the motion energy model,[40] have often been used to describe directional signals in the visual cortex,[63,66,67,70] and have been proposed to explain directional signals in the fly.[26,28,29] Interestingly, when the nonlinearity is chosen to be convex, as are most nonlinearities in these models, these models cannot generate the opponency that is observed in the decrease in mean response when a null direction sinusoid is added to a preferred direction sinusoid (Figure 4).[30]

In the fly, this same opponent phenomenon was used to suggest that dynamic nonlinearities, such as shunting currents or changing nonlinearities, were important for describing the direction-selective signals.[30] Our results show that, similarly, an LN model with a convex nonlinearity cannot describe SAC calcium responses to simple sums of sinusoids. What other properties might be required to describe these responses? First, the nonlinearity could saturate, though such models are still difficult to fit into this sort of data.[30] Second, as in the fly,[28,31] there could be shunting interactions among currents that make the voltage less linear when large amplitude stimuli are used. Third, some rectification of input signals, before the linear filtering step, can create opponent signals of the sort we observe.[65] Fourth, early visual contrast adaptation[71,72] could make LN models poor for describing responses to high contrast or natural stimuli. Note that early visual contrast adaptation exists in the fly eye,[73,74] but experiments excluded this explanation for opponency in the fly.[30] Last, it is possible that this opponency arises from inhibition from reciprocally connected SACs with opposite directional tuning.[12,75] The mechanisms for this sort of opponency seem likely to be different in fly and SAC, but this opponent phenomenon in primary directional cells can in principle improve directional signals in natural scenes, where there are strong spatial correlations in intensity.[30]

In the fly, the HS neurons downstream of T4 and T5 cells receive excitatory and inhibitory inputs from populations of cells with opposite tuning, resulting in opponent responses.[76] DSGCs downstream of SACs similarly receive excitation with mild tuning in their preferred direction and inhibition with tuning to their null direction.[16,77] The DSGCs should likewise show some opponency, and could inherit opponency from the SACs.

Generating oriented linear filters

In both T4 cells and SACs, the oriented structure of the linear filter in thought to arise from different kinetics in the inputs to the cells from different visual positions. In particular, the inputs to T4 at different spatial locations have different response dynamics,[22,24] and specific ion channels in the neurons upstream of T4 have been implicated in their response dynamics and in the tuning of T4 cells.[78] In the mouse, different bipolar cell types have different response dynamics and their postsynaptic interactions contribute to the orientation of the linear filter.[9] The origins of these temporal differences are incompletely understood but are known to involve differences both at the level of the glutamatergic input to the bipolar cell dendrite[79] and presynaptic inhibitory input to the bipolar cell axon terminal.[80]

Sequential nonlinearities to generate direction selectivity

A nonlinearity is required to generate signals that have, on average, different values for stimuli moving in opposite directions.[40,41] This means that, for instance, an oriented linear filter as in Figure 3 is by itself insufficient to generate direction-selective signals, since the *mean* filtered signal is the same for motion in both directions. In fact, any operation that extracts direction-selective signals from this linear processing necessarily contains a nonlinearity. For example, studies have measured direction selectivity using a signal's maximum value (a nonlinear operation) or its mean amplitude (which requires finding the max and min), which assume a downstream process that performs a nonlinearity.

In both fly T4 and mouse ON and OFF SACs, there appear to be several nonlinearities that contribute to direction selectivity. In fly DS cells, nonlinear shunting interactions between excitatory and inhibitory currents create some direction selectivity and can explain other direction-selective response properties of the cells.[28,30,31] However, the subsequent transformation from voltage into calcium signal applies a nonlinearity much like the point-nonlinearity in motion-energy models,[40] and this nonlinearity has been suggested to contribute to directional responses as well.[26,29,30,32,65] The transformation from calcium concentration to neurotransmitter release likely adds yet another nonlinearity that enhances directionality.[81]

A comparable suite of sequential nonlinearities acts on motion signals in the mouse retina. In the mouse SAC, as in the fly, the voltage signals are largely linear functions of the visual stimulus.[9] The transformation from voltage into changes in calcium concentration generates the directional signals we observe here (Figures 4 and 5). The transformation from calcium to synaptic release could further affect directionality, and reciprocal inhibition between SAC neurites with opposite directional tuning means that this could have complex effects.[13] Differences between flies and mice in these nonlinearities could provide mechanisms for the different degree of directionality in SACs compared to T4 cells. Another nonlinear operation occurs downstream of SACs when DS retinal ganglion cells fire action potentials.[82] This step in particular could account for why SACs have lower direction selectivity than T4 cells ($\sim$0.2 vs. 0.8; Figure 4) and direction selectivity is 2–3-fold greater in DS ganglion cells, $\sim$0.3–0.8.[59]

In comparing the direction selectivity in SACs and T4 cells (Figure 5E), it is important to consider the nonlinearity of the calcium indicators, which are different in the respective recordings. Our simulations of the two calcium indicators (Figure 2) show that indicators' responses to sinusoidal changes in calcium concentration depend on both the basal calcium level and the amplitude of the concentration changes, both within and between indicators. Thus, some of the differences in direction selectivity that we observed may reflect differences in cellular calcium concentrations or result from using different indicators.

It is notable that calcium level is not the final step in signal transduction in the cell. Indeed, calcium must be transformed into synaptic release rates, which could occur with different thresholds and kinetics in different cell types. This transduction process is also strongly nonlinear.[81] Thus, even if calcium levels were identical in SACs and T4s, the synaptic release could look quite different, thus endowing the cells with what appear to be different algorithms for processing inputs. While we believe it is useful to examine and compare calcium signals in these two cells, our measurements are at just one point in a sequence of nonlinear transformations that create motion signals to guide behavior. Subsequent processing steps could elaborate differently on similar signals or transform different signals to make them more similar. Thus, our analysis is asking the specific question of whether calcium signals are similarly constructed in these two cells, rather than whether algorithmic processing is similar across their entire computational networks. Knowing the full suite of nonlinearities downstream of calcium concentration will be important to understanding direction selectivity in graded potential release cells like these.

Natural scenes and optimization

An appealing theory about visual systems is that they have evolved to perform well with the specific statistics of their natural inputs.[83–85] Such a theory could explain similarities between mice and flies if they have evolved similar algorithms to perform motion detection in environments with similar, terrestrial visual statistics. In both the mouse and the fly visual systems, cells are solving the problem of detecting local motion. Both systems use parallel detectors tuned to respond to light and dark moving edges. This separation into distinct ON- and OFF-motion pathways has been suggested in the fly to be tuned to take advantage of the light-dark asymmetric statistics of natural scenes.[49,68,86,87] Mouse retina shows a related tuning to natural scene asymmetries.[88] The study here focused on simple visual stimuli and sensitivity to pairwise correlations as motion cues. However, studies in vertebrates and invertebrates have suggested that the combination of the two pathways, which together drive behavior, is tuned to naturalistic motion cues,[42,87,89–91] which we have not addressed in this study. In both the mouse and fly literature, there are relatively few studies of cellular responses to naturalistic motion stimuli[49,92,93] and those responses can be difficult to interpret.[94]

By directly comparing the mouse and fly primary motion detectors, we identified both commonalities and differences. The commonalities may shed light on what aspects of each system are strongly constrained by biology and the statistics of natural motion. Similarities emphasized here include receptive field structure (Figure 3), sensitivity to fast pairwise spatiotemporal correlations (Figure 4), temporal frequency tuning (Figure 5), and opponency (Figure 6). These similarities could reflect optimized algorithms that have utility over a broad range of inputs and are insensitive to the details of the implementation.

Alternatively, similarities could reflect that mice and flies solve similar problems because the statistics of their visual input are similar. Visual resolution in the fly is roughly 0.1 cpd compared to 0.5 cpd in mouse, as measured by optomotor and optokinetic behaviors and by photoreceptor acceptance angles,[57,95–99] notwithstanding suggestions of mechanisms for higher resolution in the fly.[98] Natural scene statistics may be scale free,[100] in which case this resolution difference may not much alter the filtered scene statistics. It seems likely that much visual motion is generated by self-motion, as animals translate through the world or rotate in it. Walking flies rotate at typical angular velocities of $\sim$100°/s[101,102] and higher speeds while flying[103,104]; mice rotate at typical angular velocities of 70-150°/s.[105] This means that rotations may result in similar angular speeds on the retina, though the situation is complicated by stabilizing eye and head movements in both animals.[106,107]

Translational speeds in the two animals are quite different: mice walk at up to 1 m/s and flies typically walk near 0.02 m/s but both speeds are ~10 body lengths per second.[108] Typical angular speeds across the retina depend on the animal's translational velocity divided by the distance to visual objects. If body length reflects typical distance to the ground, then the observed ground speed across the retina, in degrees per second, may not be very different between the animals. Flies fly much faster than they walk but, when flying, are also further from visual objects. Thus it remains less clear what typical visual velocities are in flight. The similarities in the algorithm we observed between mice and flies may reflect these similarities in typical retinal velocities. Ultimately, to connect algorithms in each animal to performance, we need to know more about the natural environmental statistics of each animal, as well as how those statistics depend on typical behaviors.

The differences between the two systems point to where the systems may be engaged in different goals, sensitive to different natural inputs, or differently constrained by biology. Thus, they offer interesting features to examine to understand how motion signals are processed by downstream circuits and used to drive behavior. This study highlights two substantial differences between T4 and ON SAC response properties. First, T4 neurons appear to be more direction selective in response to sinusoids than the ON SACs; postsynaptic mechanisms in mouse may allow retinal ganglion cells to "catch up" by increasing selectivity, as noted previously (Figure 5). The SACs also appear to be more broadly tuned to different spatiotemporal frequencies. Both phenomena could be due to the relative strength of non-directional excitatory inputs[16] or due to differences in how neighboring cells synapse onto one another.[12,22] The higher direction selectivity of T4 cells could also be contributed to by its OFF-channel disinhibitory input, which can amplify signals[109] and help generate opponency[30] that suppresses non-direction selective responses. Second, T4 cells responded to a smaller set of light-dark pairings during apparent motion presentations (Figure 7). In these experiments, the SACs responded to the position of the light bar in each combination, which would be consistent with their lower direction selectivity.

Same functions, different parts

Flies and mice diverged many hundred million years ago.[110] This means that similarities are likely to be the result of convergent evolution, in which motion circuits solving similar tasks evolved similar algorithms to solve them. In both flies and mice, these primary motion detectors appear integral to optic flow detection.[111–113] But they seem likely to contribute to other downstream motion computations as well, so their performance may have to be evaluated in a broad range of motion computations.

A major problem in neuroscience is to determine which features of a system are important for distinct aspects of its function. Comparative studies provide clues about which features may be universal and which may be species specific. Fly and mouse motion detectors come with very different parts lists but some similar functional properties. Here, direct comparisons have shown just how close the algorithms in these analogous circuits are but have also identified differences between them. Overall, this comparison suggests that there may exist a relatively limited set of motion detection algorithms that perform well and are consistent with biological mechanisms, even as many different mechanisms can implement them.

STAR★METHODS

Detailed methods are provided in the online version of this paper and include the following:

- KEY RESOURCES TABLE
- RESOURCE AVAILABILITY
  - Lead contact
  - Materials availability
  - Data and code availability
- EXPERIMENTAL MODEL AND STUDY PARTICIPANT DETAILS
- METHOD DETAILS
  - Starburst amacrine cell recordings
  - Visual stimulation
  - Visual stimuli
  - Calcium indicator simulations
- QUANTIFICATION AND STATISTICAL ANALYSIS
  - Imaging analysis
  - Statistics
  - Drosophila T4 recordings

SUPPLEMENTAL INFORMATION

Supplemental information can be found online at https://doi.org/10.1016/j.isci.2023.107928.

ACKNOWLEDGMENTS

AUTHOR CONTRIBUTIONS

J.C., D.A.C., and B.G.B. conceived of experiments. J.W.F. and B.G.B. acquired and analyzed mouse data. E.S.G. acquired new fly data. J.C. analyzed data. C.M.G. performed calcium indicator simulations. J.C., C.M.G., D.A.C., and B.G.B. wrote the manuscript.

DECLARATION OF INTERESTS

The authors declare no competing interests.

REFERENCES

1. Mauss, A.S., Vlasits, A., Borst, A., and Feller, M. (2017). Visual circuits for direction selectivity. Annu. Rev. Neurosci. 40, 211–230.
2. Sanes, J.R., and Zipursky, S.L. (2010). Design principles of insect and vertebrate visual systems. Neuron 66, 15–36.
3. Borst, A., and Helmstaedter, M. (2015). Common circuit design in fly and mammalian motion vision. Nat. Neurosci. 18, 1067–1076.
4. Clark, D.A., and Demb, J.B. (2016). Parallel computations in insect and mammalian visual motion processing. Curr. Biol. 26, R1062–R1072.
5. Marr, D., and Poggio, T. (1976). From Understanding Computation to Understanding Neural Circuitry (Massachussetts Institute of Technology).
6. Euler, T., Detwiler, P.B., and Denk, W. (2002). Directionally selective calcium signals in dendrites of starburst amacrine cells. Nature 418, 845–852.
7. Famiglietti, E.V., Jr. (1983). On and off pathways through amacrine cells in mammalian retina: the synaptic connections of "starburst" amacrine cells. Vision Res. 23, 1265–1279.
8. Briggman, K.L., Helmstaedter, M., and Denk, W. (2011). Wiring specificity in the direction-selectivity circuit of the retina. Nature 471, 183–188.
9. Fransen, J.W., and Borghuis, B.G. (2017). Temporally Diverse Excitation Generates Direction-Selective Responses in ON-and OFF-Type Retinal Starburst Amacrine Cells. Cell Rep. 18, 1356–1365.
10. Kim, J.S., Greene, M.J., Zlateski, A., Lee, K., Richardson, M., Turaga, S.C., Purcaro, M., Balkam, M., Robinson, A., Behabadi, B.F., et al. (2014). Space-time wiring specificity supports direction selectivity in the retina. Nature 509, 331–336.
11. Greene, M.J., Kim, J.S., and Seung, H.S.; EyeWirers (2016). Analogous convergence of sustained and transient inputs in parallel on and off pathways for retinal motion computation. Cell Rep. 14, 1892–1900.
12. Lee, S., and Zhou, Z.J. (2006). The synaptic mechanism of direction selectivity in distal processes of starburst amacrine cells. Neuron 51, 787–799.
13. Chen, Q., Pei, Z., Koren, D., and Wei, W. (2016). Stimulus-dependent recruitment of lateral inhibition underlies retinal direction selectivity. Elife 5, e21053.
14. Pei, Z., Chen, Q., Koren, D., Giammarinaro, B., Acaron Ledesma, H., and Wei, W. (2015). Conditional knock-out of vesicular GABA transporter gene from starburst amacrine cells reveals the contributions of multiple synaptic mechanisms underlying direction selectivity in the retina. J. Neurosci. 35, 13219–13232.
15. Haussel, S.E., Euler, T., Detwiler, P.B., and Denk, W. (2007). A dendrite-autonomous mechanism for direction selectivity in retinal starburst amacrine cells. PLoS Biol. 5, e185.
16. Matsumoto, A., Agbariah, W., Nolte, S.S., Andrawos, R., Levi, H., Sabbah, S., and Yonehara, K. (2021). Direction selectivity in retinal bipolar cell axon terminals. Neuron 109, 3895–3896.
17. Sethuramanujam, S., McLaughlin, A.J., Hoggarth, A., Schwab, D.J., and Awatramani, G.B. (2016). A central role for mixed acetylcholine/GABA transmission in direction coding in the retina. Neuron 90, 1–14.
18. Agrochao, M., Tanaka, R., Salazar-Gatzimas, E., and Clark, D.A. (2020). Mechanism for analogous illusory motion perception in flies and humans. Proc. Natl. Acad. Sci. USA 117, 23044–23053.
19. Maisak, M.S., Haag, J., Ammer, G., Serbe, E., Meier, M., Leonhardt, A., Schilling, T., Bahl, A., Rubin, G.M., Nern, A., et al. (2013). A directional tuning map of Drosophila elementary motion detectors. Nature 500, 212–216.
20. Behnia, R., Clark, D.A., Carter, A.G., Clandinin, T.R., and Desplan, C. (2014). Processing properties of ON and OFF pathways for Drosophila motion detection. Nature 512, 427–430.
21. Strother, J.A., Wu, S.-T., Wong, A.M., Nern, A., Rogers, E.M., Le, J.Q., Rubin, G.M., and Reiser, M.B. (2017). The emergence of directional selectivity in the visual motion pathway of Drosophila. Neuron 94, 168–182.e10.
22. Takemura, S.-Y., Aso, Y., Hige, T., Wong, A., Lu, Z., Xu, C.S., Rivlin, P.K., Hess, H., Zhao, T., Parag, T., et al. (2017). The comprehensive connectome of a neural substrate for 'ON' motion detection in Drosophila. Elife 6, e26975.
23. Shinomiya, K., Huang, G., Lu, Z., Parag, T., Xu, C.S., Aniceto, R., Ansari, N., Cheatham, N., Lauchie, S., Neace, E., et al. (2019). Comparisons between the ON-and OFF-edge motion pathways in the Drosophila brain. Elife 8, e40025.
24. Arenz, A., Drews, M.S., Richter, F.G., Ammer, G., and Borst, A. (2017). The temporal tuning of the Drosophila motion detectors is determined by the dynamics of their input elements. Curr. Biol. 27, 929–944.
25. Strother, J., Nern, A., and Reiser, M. (2014). Direct observation of ON and OFF pathways in the Drosophila visual system. Curr. Biol. 24, 976–983.
26. Leong, J.C.S., Esch, J.J., Poole, B., Ganguli, S., and Clandinin, T.R. (2016). Direction selectivity in Drosophila emerges from preferred-direction enhancement and null-direction suppression. J. Neurosci. 36, 8078–8092.
27. Salazar-Gatzimas, E., Chen, J., Creamer, M.S., Mano, O., Mandel, H.B., Matulis, C.A., Pottackal, J., and Clark, D.A. (2016). Direct measurement of correlation responses in Drosophila elementary motion detectors reveals fast timescale tuning. Neuron 92, 227–239.
28. Gruntman, E., Romani, S., and Reiser, M.B. (2018). Simple integration of fast excitation and offset, delayed inhibition computes directional selectivity in Drosophila. Nat. Neurosci. 21, 250–257.
29. Wienecke, C.F.R., Leong, J.C.S., and Clandinin, T.R. (2018). Linear Summation Underlies Direction Selectivity in Drosophila. Neuron 99, 680–688.e4.
30. Badwan, B.A., Creamer, M.S., Zavatone-Veth, J.A., and Clark, D.A. (2019). Dynamic nonlinearities enable direction opponency in Drosophila elementary motion detectors. Nat. Neurosci. 22, 1318–1326.
31. Gruntman, E., Romani, S., and Reiser, M.B. (2019). The computation of directional selectivity in the Drosophila OFF motion pathway. Elife 8, e50706.
32. Mishra, A., Serbe-Kamp, E., Borst, A., and Haag, J. (2023). Voltage to calcium transformation enhances direction selectivity in Drosophila T4 neurons. J. Neurosci. 43, 2497–2514.
33. Poleg-Polsky, A., Ding, H., and Diamond, J.S. (2018). Functional compartmentalization within starburst

amacrine cell dendrites in the retina. Cell Rep. *22*, 2898–2908.

34. Chen, T.-W., Wardill, T.J., Sun, Y., Pulver, S.R., Renninger, S.L., Baohan, A., Schreiter, E.R., Kerr, R.A., Orger, M.B., Jayaraman, V., et al. (2013). Ultrasensitive fluorescent proteins for imaging neuronal activity. Nature *499*, 295–300.

35. Sun, X.R., Badura, A., Pacheco, D.A., Lynch, L.A., Schneider, E.R., Taylor, M.P., Hogue, I.B., Enquist, L.W., Murthy, M., and Wang, S.S.-H. (2013). Fast GCaMPs for improved tracking of neuronal activity. Nat. Commun. *4*, 2170.

36. Badura, A., Sun, X.R., Giovannucci, A., Lynch, L.A., and Wang, S.S.-H. (2014). Fast calcium sensor proteins for monitoring neural activity. Neurophotonics *1*, 025008.

37. Hendel, T., Mank, M., Schnell, B., Griesbeck, O., Borst, A., and Reiff, D.F. (2008). Fluorescence changes of genetic calcium indicators and OGB-1 correlated with neural activity and calcium in vivo and in vitro. J. Neurosci. *28*, 7399–7411.

38. Chichilnisky, E.J. (2001). A simple white noise analysis of neuronal light responses. Network: Comput. Neural Syst. *12*, 199–213.

39. Marmarelis, V.Z. (2004). Nonlinear Dynamic Modeling of Physiological Systems (IEEE Press).

40. Adelson, E.H., and Bergen, J.R. (1985). Spatiotemporal energy models for the perception of motion. JOSA A *2*, 284–299.

41. Borst, A., and Egelhaaf, M. (1989). Principles of visual motion detection. Trends Neurosci. *12*, 297–306.

42. Fitzgerald, J.E., Katsov, A.Y., Clandinin, T.R., and Schnitzer, M.J. (2011). Symmetries in stimulus statistics shape the form of visual motion estimators. Proc. Natl. Acad. Sci. USA *108*, 12909–12914.

43. Potters, M., and Bialek, W. (1994). Statistical mechanics and visual signal processing. J. Phys. *4*, 1755–1775.

44. van Steveninck, R., Bialek, W., Potters, M., Carlson, R., and Lewen, G. (1995). Adaptive Movement Computation in the Blowfly Visual System (Pion LTD), p. 99.

45. Roy, S., and de Ruyter van Steveninck, R. (2016). Bilocal visual noise as a probe of wide field motion computation. J. Vis. *16*, 8.

46. Anstis, S.M. (1970). Phi movement as a subtraction process. Vision Res. *10*, 1411–1430.

47. Bours, R.J.E., Kroes, M.C.W., and Lankheet, M.J. (2009). Sensitivity for reverse-phi motion. Vision Res. *49*, 1–9.

48. Hassenstein, B., and Reichardt, W. (1956). Systemtheoretische Analyse der Zeit-Reihenfolgen-und Vorzeichenauswertung bei der Bewegungsperzeption des Rüsselkäfers Chlorophanus. Z. Naturforsch. *11*, 513–524.

49. Salazar-Gatzimas, E., Agrochao, M., Fitzgerald, J.E., and Clark, D.A. (2018). The Neuronal Basis of an Illusory Motion Percept Is Explained by Decorrelation of Parallel Motion Pathways. Curr. Biol. *28*, 3748–3762.e8.

50. Kirkels, L.A.M.H., Zhang, W., Duijnhouwer, J., and van Wezel, R.J.A. (2020). Opto-locomotor reflexes of mice to reverse-phi stimuli. J. Vis. *20*, 7.

51. van Hateren, J.H., and Snippe, H.P. (2006). Phototransduction in primate cones and blowfly photoreceptors: different mechanisms, different algorithms, similar response. J. Comp. Physiol. *192*, 187–197.

52. Daly, S.J., and Normann, R.A. (1985). Temporal information processing in cones: effects of light adaptation on temporal summation and modulation. Vision Res. *25*, 1197–1206.

53. Howard, J., Dubs, A., and Payne, R. (1984). The dynamics of phototransduction in insects. J. Comp. Physiol. *154*, 707–718.

54. Creamer, M.S., Mano, O., and Clark, D.A. (2018). Visual Control of Walking Speed in Drosophila. Neuron *100*, 1460–1473.e6.

55. Priebe, N.J., Lisberger, S.G., and Movshon, J.A. (2006). Tuning for spatiotemporal frequency and speed in directionally selective neurons of macaque striate cortex. J. Neurosci. *26*, 2941–2950.

56. Reichardt, W., and Varju, D. (1959). Übertragungseigenschaften im Auswertesystem für das Bewegungssehen:(Folgerungen aus Experimenten an dem Rüsselkäfer Chlorophanus viridis). Z. Naturforsch. B Chem. Sci. *14*, 674–689.

57. Buchner, E. (1976). Elementary movement detectors in an insect visual system. Biol. Cybern. *24*, 85–101.

58. Fried, S.I., Münch, T.A., and Werblin, F.S. (2005). Directional selectivity is formed at multiple levels by laterally offset inhibition in the rabbit retina. Neuron *46*, 117–127.

59. Wei, W., Hamby, A.M., Zhou, K., and Feller, M.B. (2011). Development of asymmetric inhibition underlying direction selectivity in the retina. Nature *469*, 402–406.

60. Jain, V., Murphy-Baum, B.L., deRosenroll, G., Sethuramanujam, S., Delsey, M., Delaney, K.R., and Awatramani, G.B. (2020). The functional organization of excitation and inhibition in the dendrites of mouse direction-selective ganglion cells. Elife *9*, e52949.

61. Taylor, W.R., and Smith, R.G. (2012). The role of starburst amacrine cells in visual signal processing. Vis. Neurosci. *29*, 73–81.

62. Taylor, W.R., He, S., Levick, W.R., and Vaney, D.I. (2000). Dendritic computation of direction selectivity by retinal ganglion cells. Science *289*, 2347–2350.

63. Jagadeesh, B., Wheat, H.S., and Ferster, D. (1993). Linearity of summation of synaptic potentials underlying direction selectivity in simple cells of the cat visual cortex. Science *262*, 1901–1904.

64. Heeger, D.J., Boynton, G.M., Demb, J.B., Seidemann, E., and Newsome, W.T. (1999). Motion opponency in visual cortex. J. Neurosci. *19*, 7162–7174.

65. Zavatone-Veth, J.A., Badwan, B.A., and Clark, D.A. (2020). A minimal synaptic model for direction selective neurons in Drosophila. J. Vis. *20*, 2.

66. Lien, A.D., and Scanziani, M. (2018). Cortical direction selectivity emerges at convergence of thalamic synapses. Nature *1*.

67. Heeger, D.J. (1992). Half-squaring in responses of cat striate cells. Vis. Neurosci. *9*, 427–443.

68. Mano, O., Creamer, M.S., Badwan, B.A., and Clark, D.A. (2021). Predicting individual neuron responses with anatomically constrained task optimization. Curr. Biol. *31*, 4062–4075.e4.

69. Haag, J., Arenz, A., Serbe, E., Gabbiani, F., and Borst, A. (2016). Complementary mechanisms create direction selectivity in the fly. Elife *5*, e17421. https://doi.org/10.7554/eLife.17421.

70. Priebe, N.J., and Ferster, D. (2006). Mechanisms underlying cross-orientation suppression in cat visual cortex. Nat. Neurosci. *9*, 552–561.

71. Rieke, F. (2001). Temporal contrast adaptation in salamander bipolar cells. J. Neurosci. *21*, 9445–9454.

72. Baccus, S.A., and Meister, M. (2002). Fast and slow contrast adaptation in retinal circuitry. Neuron *36*, 909–919.

73. Matulis, C.A., Chen, J., Gonzalez-Suarez, A.D., Behnia, R., and Clark, D.A. (2020). Heterogeneous temporal contrast adaptation in Drosophila direction-selective circuits. Curr. Biol. *30*, 222–236.e6.

74. Drews, M.S., Leonhardt, A., Pirogova, N., Richter, F.G., Schuetzenberger, A., Braun, L., Serbe, E., and Borst, A. (2020). Dynamic Signal Compression for Robust Motion Vision in Flies. Curr. Biol. *30*, 209–221.e8.

75. Ding, H., Smith, R.G., Poleg-Polsky, A., Diamond, J.S., and Briggman, K.L. (2016). Species-specific wiring for direction selectivity in the mammalian retina. Nature *535*, 105–110.

76. Mauss, A.S., Pankova, K., Arenz, A., Nern, A., Rubin, G.M., and Borst, A. (2015). Neural circuit to integrate opposing motions in the visual field. Cell *162*, 351–362.

77. Vaney, D.I., Sivyer, B., and Taylor, W.R. (2012). Direction selectivity in the retina: symmetry and asymmetry in structure and function. Nat. Rev. Neurosci. *13*, 194–208.

78. Gonzalez-Suarez, A.D., Zavatone-Veth, J.A., Chen, J., Matulis, C.A., Badwan, B.A., and Clark, D.A. (2022). Excitatory and inhibitory neural dynamics jointly tune motion detection. Curr. Biol. *32*, 3659–3675.e8.

79. DeVries, S.H., Li, W., and Saszik, S. (2006). Parallel processing in two transmitter microenvironments at the cone photoreceptor synapse. Neuron *50*, 735–748.

80. Franke, K., Berens, P., Schubert, T., Bethge, M., Euler, T., and Baden, T. (2017). Inhibition decorrelates visual feature representations in the inner retina. Nature *542*, 439–444.

81. Neher, E., and Sakaba, T. (2008). Multiple roles of calcium ions in the regulation of neurotransmitter release. Neuron *59*, 861–872.

82. Oesch, N., Euler, T., and Taylor, W.R. (2005). Direction-selective dendritic action potentials in rabbit retina. Neuron *47*, 739–750.

83. Simoncelli, E.P., and Olshausen, B.A. (2001). Natural image statistics and neural representation. Annu. Rev. Neurosci. *24*, 1193–1216.

84. Laughlin, S. (1981). A simple coding procedure enhances a neuron's information capacity. Z. Naturforsch. *36*, 910–912.

85. Srinivasan, M.V., Laughlin, S.B., and Dubs, A. (1982). Predictive coding: a fresh view of inhibition in the retina. Proc. R. Soc. Lond. B Biol. Sci. *216*, 427–459.

86. Leonhardt, A., Ammer, G., Meier, M., Serbe, E., Bahl, A., and Borst, A. (2016). Asymmetry of Drosophila ON and OFF motion detectors enhances real-world velocity estimation. Nat. Neurosci. *19*, 706–715.

87. Clark, D.A., Fitzgerald, J.E., Ales, J.M., Gohl, D.M., Silies, M.A., Norcia, A.M., and Clandinin, T.R. (2014). Flies and humans share a motion estimation strategy that exploits natural scene statistics. Nat. Neurosci. *17*, 296–303.

88. Ratliff, C.P., Borghuis, B.G., Kao, Y.-H., Sterling, P., and Balasubramanian, V. (2010).

Retina is structured to process an excess of darkness in natural scenes. Proc. Natl. Acad. Sci. USA *107*, 17368–17373.

89. Fitzgerald, J.E., and Clark, D.A. (2015). Nonlinear Circuits for Naturalistic Visual Motion Estimation. eLifee09123.

90. Yildizoglu, T., Riegler, C., Fitzgerald, J.E., and Portugues, R. (2020). A Neural Representation of Naturalistic Motion-Guided Behavior in the Zebrafish Brain. Curr. Biol. *30*, 2321–2333.e6.

91. Chen, J., Mandel, H.B., Fitzgerald, J.E., and Clark, D.A. (2019). Asymmetric ON-OFF processing of visual motion cancels variability induced by the structure of natural scenes. Elife *8*, e47579.

92. Straw, A.D., Rainsford, T., and O'Carroll, D.C. (2008). Contrast sensitivity of insect motion detectors to natural images. J. Vis. *8*, 32.

93. Cafaro, J., Zylberberg, J., and Field, G.D. (2020). Global motion processing by populations of direction-selective retinal ganglion cells. J. Neurosci. *40*, 5807–5819.

94. Sharpee, T., Rust, N.C., and Bialek, W. (2004). Analyzing neural responses to natural signals: maximally informative dimensions. Neural Comput. *16*, 223–250.

95. Stavenga, D.G. (2003). Angular and spectral sensitivity of fly photoreceptors. II. Dependence on facet lens F-number and rhabdomere type in Drosophila. J. Comp. Physiol. A Neuroethol. Sens. Neural Behav. Physiol. *189*, 189–202.

96. Prusky, G.T., West, P.W., and Douglas, R.M. (2000). Behavioral assessment of visual acuity in mice and rats. Vision Res. *40*, 2201–2209.

97. Götz, K. (1964). Optomotorische untersuchung des visuellen systems einiger augenmutanten der fruchtfliege Drosophila. Biol. Cybern. *2*, 77–92.

98. Juusola, M., Dau, A., Song, Z., Solanki, N., Rien, D., Jaciuch, D., Dongre, S.A., Blanchard, F., de Polavieja, G.G., Hardie, R.C., and Takalo, J. (2017). Microsaccadic sampling of moving image information provides Drosophila hyperacute vision. Elife *6*, e26117.

99. Tokashiki, N., Nishiguchi, K.M., Fujita, K., Sato, K., Nakagawa, Y., and Nakazawa, T.

(2018). Reliable detection of low visual acuity in mice with pattern visually evoked potentials. Sci. Rep. *8*, 15948.

100. Ruderman, D.L., and Bialek, W. (1994). Statistics of natural images: Scaling in the woods. Phys. Rev. Lett. *73*, 814–817.

101. DeAngelis, B.D., Zavatone-Veth, J.A., and Clark, D.A. (2019). The manifold structure of limb coordination in walking Drosophila. Elife *8*, e46409.

102. Katsov, A.Y., Freifeld, L., Horowitz, M., Kuehn, S., and Clandinin, T.R. (2017). Dynamic structure of locomotor behavior in walking fruit flies. Elife *6*, e26410.

103. Muijres, F.T., Elzinga, M.J., Melis, J.M., and Dickinson, M.H. (2014). Flies evade looming targets by executing rapid visually directed banked turns. Science *344*, 172–177.

104. Muijres, F.T., Elzinga, M.J., Iwasaki, N.A., and Dickinson, M.H. (2015). Body saccades of Drosophila consist of stereotyped banked turns. J. Exp. Biol. *218*, 864–875.

105. Meyer, A.F., Poort, J., O'Keefe, J., Sahani, M., and Linden, J.F. (2018). A head-mounted camera system integrates detailed behavioral monitoring with multichannel electrophysiology in freely moving mice. Neuron *100*, 46–60.e7.

106. Meyer, A.F., O'Keefe, J., and Poort, J. (2020). Two distinct types of eye-head coupling in freely moving mice. Curr. Biol. *30*, 2116–2130.e6.

107. Fenk, L.M., Avritzer, S.C., Weisman, J.L., Nair, A., Randt, L.D., Mohren, T.L., Siwanowicz, I., and Maimon, G. (2022). Muscles that move the retina augment compound eye vision in Drosophila. Nature *612*, 116–122.

108. Gonçalves, A.I., Zavatone-Veth, J.A., Carey, M.R., and Clark, D.A. (2022). Parallel locomotor control strategies in mice and flies. Curr. Opin. Neurobiol. *73*, 102516.

109. Groschner, L.N., Malis, J.G., Zuidinga, B., and Borst, A. (2022). A biophysical account of multiplication by a single neuron. Nature *603*, 119–123.

110. Peterson, K.J., Lyons, J.B., Nowak, K.S., Takacs, C.M., Wargo, M.J., and McPeek, M.A. (2004). Estimating metazoan divergence times with a molecular clock. Proc. Natl. Acad. Sci. USA *101*, 6536–6541.

111. Krapp, H.G., and Hengstenberg, R. (1996). Estimation of self-motion by optic flow processing in single visual interneurons. Nature *384*, 463–466.

112. Sabbah, S., Gemmer, J.A., Bhatia-Lin, A., Manoff, G., Castro, G., Siegel, J.K., Jeffery, N., and Berson, D.M. (2017). A retinal code for motion along the gravitational and body axes. Nature *546*, 492–497.

113. Henning, M., Ramos-Traslosheros, G., Gür, B., and Silies, M. (2022). Populations of local direction–selective cells encode global motion patterns generated by self-motion. Sci. Adv. *8*, eabi7112.

114. Pologruto, T.A., Sabatini, B.L., and Svoboda, K. (2003). ScanImage: flexible software for operating laser scanning microscopes. Biomed. Eng. Online *2*, 13.

115. Kleiner, M., Brainard, D., Pelli, D., Ingling, A., Murray, R., and Broussard, C. (2007). What's new in Psychtoolbox-3. Perception *36*, 1.

116. Brainard, D.H. (1997). The psychophysics toolbox. Spatial Vis. *10*, 433–436.

117. Pelli, D.G. (1997). The VideoToolbox software for visual psychophysics: Transforming numbers into movies. Spatial Vis. *10*, 437–442.

118. Creamer, M.S., Mano, O., Tanaka, R., and Clark, D.A. (2019). A flexible geometry for panoramic visual and optogenetic stimulation during behavior and physiology. J. Neurosci. Methods *323*, 48–55.

119. van Steveninck, R., Bialek, W., Potters, M., Carlson, R., and Lewen, G. (1996). Adaptive Movement Computation by the Blowfly Visual System (SIAM), p. 21.

120. Reingruber, J., Ingram, N.T., Griffis, K.G., and Fain, G.L. (2020). A kinetic analysis of mouse rod and cone photoreceptor responses. J. Physiol. *598*, 3747–3763.

121. Umino, Y., Solessio, E., and Barlow, R.B. (2008). Speed, spatial, and temporal tuning of rod and cone vision in mouse. J. Neurosci. *28*, 189–198.

122. Juusola, M., and Hardie, R.C. (2001). Light Adaptation in Drosophila Photoreceptors I. Response Dynamics and Signaling Efficiency at 25° C. J. Gen. Physiol. *117*, 3–25.

STAR★METHODS

KEY RESOURCES TABLE

REAGENT or RESOURCE	SOURCE	IDENTIFIER
Chemicals, peptides, and recombinant proteins		
Oregon Green 488 Bapta-1 (OGB-1), Hexapotassium Salt, cell impermeant	ThermoFisher Sci.	O-6806
Ames Medium	Sigma-Aldrich	A1420
Experimental models: Organisms/strains		
ChAT-IRES-Cre mouse	Jackson Laboratory	RRID:IMSR_JAX:006410
CAG-tdTomato (Ai9) mouse	Jackson Laboratory	RRID:IMSR_JAX:007905
Software and algorithms		
MATLAB R2022a	The Mathworks	v.9.12.0.1956245 Update 2
SAC calcium imaging data	DataDryad.org	https://doi.org/10.5061/dryad.sj3tx969p
MATLAB code for data analysis and visualization	GitHub.com	github.com/ClarkLabCode/StarburstAnalysisPub.

RESOURCE AVAILABILITY

Lead contact

Requests for further information should be directed to the lead contact, Bart Borghuis (bart.borghuis@louisville.edu).

Materials availability

This study did not generate new unique reagents.

Data and code availability

- Starburst amacrine cell recording data used in this study has been deposited at DataDryad.org and are publicly available as of the date of publication. The DOI is listed in the key resources table.
- Code to analyze that data and create the figures in this study has been deposited at Github.com. The accession numbers is listed in the key resources table.

EXPERIMENTAL MODEL AND STUDY PARTICIPANT DETAILS

All experiments were performed using offspring of transgenic ChAT-IRES-Cre mice (Jackson Laboratory; RRID: IMSR_JAX:006410) crossed with the Ai9 CAG-tdTomato ROSA26 reporter line (Jackson Laboratory; RRID: IMSR_JAX:007905). Mice of either sex, maintained on C57BL/6J backgrounds, were kept on a 12:12 light/dark schedule and studied between 1.5 and 3 months of age. We report no difference between data obtained from female and male mice and data is presented combined throughout. All animal procedures were approved by the Institutional Animal Care and Use Committee at the University of Louisville and were in compliance with National Institutes of Health guidelines.

METHOD DETAILS

Starburst amacrine cell recordings

Retina preparation and calcium imaging

Optical recordings of visually evoked calcium responses in SAC distal dendritic branches were obtained with 2P fluorescence imaging of the whole-mount mouse retina, *in vitro*. Retinas of CX57BL6/J mice of either sex (2–6 months of age) were prepared and maintained in carbogenated (95% O2–5% CO2) Ames Medium (Sigma-Aldrich) following enucleation and dissection of the eye under infrared illumination using night vision scopes (Night Vision Devices; Allentown, PA) mounted on a dissecting scope (Olympus SZ61). For recording, a retina was transferred to a chamber on the stage of an customized Olympus BX51 microscope and continuously perfused with heated, carbogenated Ames medium (∼6 mL/min; 34°C–36°C). TdTomato fluorescence-expressing SACs were located using 2P imaging and up to four SACs per retina were filled with the cell impermeant calcium indicator dye Oregon Green 488 BAPTA-1 (OGB-1 hexapotassium salt, 10 mM in dH2O; Invitrogen, Catalog number: O6806) by electroporation under visual guidance using a glass pipette (10 μL loaded volume; typical impedance 20 MΩ; −250 pA holding current; single buzz, 2 ms, followed by retraction of the pipette). Recordings were initiated 1h after completing the fills. The custom-built 2P fluorescence microscope was controlled with ScanImage v3.8.1 software (www.scanimage.org).[114]

Visual stimulation

Visual stimuli were generated with an Apple Macintosh iMac computer using custom algorithms written in MATLAB (MathWorks; Natick, MA) and the Psychophysics Toolbox (PTB-3; psychtoolbox.org).[115–117] Visual stimuli on a photopic background (λ_{max} = 395 nm; 1.2 · 10^4 R*/rod and cone/s) were displayed using a DLP video projector (HP AX325AA; Hewlett-Packard) with the image projected onto the photoreceptor layer using the microscope condenser. Stimuli were radially symmetric with a 'bullseye' geometry and were presented centered on the soma of the recorded cell.

Visual stimuli

Visual stimuli presented to SACs in this study are largely adapted from the visual stimuli presented to flies in several previous studies[27,30,49,118] but using a bullseye geometry and using different spatiotemporal parameters, tuned to the starburst cell. To minimize possible stimulus adaptation, trials were separated by 6 s of mean-gray background presentation. To exclude potential responses to scan laser onset, a 1.5 s blank period preceded the visual stimulus on each trial and the fluorescence signal during this period was excluded from the analysis.

Dark and light edges (Figure 1): Full contrast light or dark edges moved radially outward or radially inward, occluding a gray background at velocity of 500 $\mu m/s$. After the stimulus covered the entire circle, the circle remained light/dark until 3 s after the edge began to move.

Uncorrelated stochastic stimulus (Figure 3): Contrasts of each spatial location were set randomly to be +1 or −1, and they were updated every 30th of a second (parameters for all stimuli listed below).

Ternary correlated stochastic stimulus (Figure 4): This stimulus creates pairwise spatiotemporal correlations at a given spatial and temporal offset. It is identical to previously used stimuli[27] and similar to other published methods.[45,119] The contrast at each pixel in space and time was $c(x,t) = B(x,t) + P * B(x + \Delta x, t + \Delta t)$, with $P = \pm 1$ to obtain positive or negative correlations. $B(x,t)$ is a binary random variable taking the value of −0.25 and 0.25, so the contrasts take values of −0.5, 0, and 0.5 with probabilities 1/4, 1/2 and 1/4. The autocovariance of the stimulus was

$$\Phi(dx, dt) = \langle c(x+dx, t+dt)c(x,t) \rangle_{x,t} = 2\,\phi(dx, dt) + P * (\phi(dx + \Delta x, dt + \Delta t) + \phi(dx - \Delta x, dt - \Delta t)),$$

where the $\varphi(x,t)$ denotes the autocorrelation of $B(x,t)$:

$$\phi(x,t) = \begin{cases} 1/16, & \text{if } x = 0, t = 0 \\ 0, & \text{otherwise} \end{cases}.$$

P denotes the parity of the imposed correlations, and there was positive (negative) correlation between two points with spatial offset of Δx and temporal offset of Δt when P takes the value of 1 (−1). In Figure 4, we plot the autocorrelation of the stimulus where the $\Phi(0,0)$ is normalized to be 1. Δt ranged from 0 ms to 250 ms, and $\Delta x = \pm 50\,\mu m$, where positive (negative) Δx led to correlation in preferred (null) direction. The frame was updated at 20 frame per second, a rate that we found empirically drove directional responses in our recordings; faster rates seemed not to strongly drive the cells. This is consistent with the slower light responses of mouse cones[120,121] compared to fly photoreceptors[122] at the light intensity ranges of these experiments.

Sinusoidal grating stimulus (Figures 4 and 5): The stimulus has contrast $c(x,t) = A \sin(D * 2\pi f * t + 2\pi k * x)$, where the temporal frequencies f ranged from 0.5 Hz to 8 Hz, spatial frequency k ranged from 1/450 to 1/150 μm^{-1}. When $D = 1$, the gratings moved outward; when $D = -1$, the sinusoid moved inward. In Figure 5, the amplitude of the sinusoids was 1, and in Figure 5, the amplitude was 0.5.

Counter-phase grating stimulus (Figure 6): The counter-phase sinusoid gratings are the linear sum of two drifting sinusoid gratings moving in the opposite direction: $c(x,t) = 0.5 * \sin(2\pi f * t + 2\pi k * x + \phi) + 0.5 * \sin(- 2\pi f * t + 2\pi k * x + \phi)$, where the relative phase of the two sinusoids, ϕ, of the sinusoid ranged over 8 values uniformly from 0 to 2π. The temporal frequency was 2 Hz and spatial frequency was 1/150 μm^{-1}.

Apparent motion stimulus (Figure 7): Two adjacent rings were either white or black on a gray background for 1 s. The two rings were presented sequentially. The leading ring appeared 250 ms before the onset the lagging ring, and both ring disappeared after 1 s of the onset of the leading ring. When the inner (outer) ring is the leading ring, the apparent motion is defined to move in the preferred (null) direction. All contrast combinations were tested.

Single ring stimulus (Figures 1–7): A single ring that was either white or black appeared on a gray background. The bar appeared for 1 s before the screen returned to uniform gray.

The spatial and temporal scales and resolutions of visual stimuli for different experiments in starburst amacrine cells were as follows:

Visual stimulus	Figure	Radial pixel resolution (μm)	Temporal pixel resolution (s)	Stimulus radial extent (μm)	Stimulus Duration (s)
Edge stimulus	1	3.3	1/60	150	3
Uncorrelated stochastic stimulus	3	16	1/30	240	320
Ternary correlated stochastic stimulus	4	50	1/60	250	5
Sinusoidal gratings	5, 6	3.3	1/60	300	5

(Continued on next page)

Continued

Visual stimulus	Figure	Radial pixel resolution (μm)	Temporal pixel resolution (s)	Stimulus radial extent (μm)	Stimulus Duration (s)
Counter-phase sinusoidal grating	6	3.3	1/60	300	5
Apparent motion	7	50	1/60	100	1
Single ring	Figure S1	50	1/60	50	1

Calcium indicator simulations

The results shown in Figure 2 were generated by simulating simple models of calcium indicator dynamics. In these models, we characterized the calcium's fraction bound, b, by the differential equation,

$$\tau_b \dot{b} = \frac{C^n}{K_D^n} - b\left(1 + \frac{C^n}{K_D^n}\right),$$

where C is the calcium concentration, K_d is the binding constant of the indicator, and τ_b is the indicator time constant (parameter values used in the simulations listed below). This dynamical equation yields the expected steady state binding fraction in the form of a Hill function

$$b_{ss} = \frac{C^n}{K_D^n + C^n}$$

The fraction bound as a function of time was solved numerically via Euler Integration with timesteps of 0.1 ms and scaled by the dynamic range, D, the ratio of brightest to dimmest fluorescence of the indicator, to determine the florescence, F, and the fractional change in fluorescence, $\Delta F/F$:

$$F = F_{min}(1 + (D-1)b)$$

$$\frac{\Delta F}{F} = \frac{F - F_0}{F_0}$$

For our plots, F_0 is calculated as the fluorescence just before a stimulus begins. A known function, such as a sinusoid, can be used as the calcium concentration over time. To create the stochastic traces for filter extraction, we generated stimulus traces with Gaussian distributed random intensity values that update at a frequency of 200 Hz. This simulates a Gaussian distributed visual stimulus, for instance. These intensity values were then filtered by a temporal weighting function, after which the filtered signal, $s(t)$, was mean subtracted and set to have standard deviation of 1. Calcium concentration traces, $C(t)$, were set to $C(t) = C_0\left(1 + \frac{s(t)}{2}\right)$, where C_0 set the scale of the basal calcium levels and was equal to $1/3\,K_D$, K_D, or $3K_D$. Negative calcium concentrations were set to 0. The temporal weighting filter was of the form,

$$f(t) = \frac{t}{\tau^2} e^{-\frac{t}{\tau}},$$

with a time constant, τ, of 50 ms. This same procedure was performed with the spatiotemporal stimuli and filter. The spatiotemporal stimulus had uncorrelated Gaussian intensity values that varied with a 200 Hz temporal frequency at each of 21 spatial positions. The weighting filter used to generate the responses to the spatiotemporal stimuli was the sum of two outer products of Gaussian spatial filters and Gamma function integrand temporal filters. The $\Delta F/F$ traces were regressed against the original intensity to extract the linear filters of the stimulus that best predicted the response.

Parameters used for the simulations of OGB and GCaMP6f calcium indicators were as follows.

Parameter	OGB Value (citation)	GCaMP6f Value (citation)
τ, time constant	5 ms (Sun et al.[35])	254 ms (Chen et al.[34])
n, hill coefficient	1 (Badura et al.[36])	2.27 (Chen et al.[34])
K_D, dissociation constant	0.24 μM (Hendel et al.[37])	0.375 μM (Chen et al.[34])
D, dynamic range	14 (Badura et al.[36])	29.2 (Chen et al.[34])

QUANTIFICATION AND STATISTICAL ANALYSIS

Imaging analysis

Regions of interest (ROIs) were extracted from mean fluorescence image (movie averaged across time) with a watershed algorithm using custom MATLAB code. For each movie, we averaged over responses of all ROIs to generate the response to the stimulus. Light from stimulus projector leaked into the movies. We estimated the strength of the bleed-through by calculating the signal of the darkest region in a recording, and we subtracted it from the fluorescent responses.

We calculated $\Delta F/F$ with the formula $\frac{\Delta F}{F} = \frac{F - F_0}{F_0}$, where F_0 was computed to be the average fluorescent signal during the 1 s prior to stimulus onset of each trial.

To compute the linear receptive field, we first high pass filtered with a 0.1 Hz filter to remove long-time scale fluctuations in the response. We calculated the $\Delta F/F$ as before, and then performed reverse-correlation between the stimulus and response.

To compute time-averaged responses, response traces were averaged over the full duration of the stimulus, except for sinusoidal grating experiments. In those experiments, to account for phase-dependency in the responses, we averaged the responses over time intervals that were the largest integer-multiple of the sinusoid period that was still less than the stimulus duration.

We developed a simple metric to quantify the similarity between the linear receptive fields (RFs) of T4 and the ON-SAC (Figure 3). To calculate this metric, we viewed the RFs of T4 and SAC as two vectors, and measured the cosine similarities between them. We first rescaled the T4 RF with various spatiotemporal scales. For each rescaling, we calculated the cosine similarity between the vectors, interpolating in space and time when necessary. We shifted them spatially to all possible offsets and used the maximum cosine similarity over those shifts as the similarity for that spatial and temporal scaling.

Statistics

In the starburst data, we treated each dendritic branch recording as a statistically independent data point. Statistical significances were calculated with Wilcoxon signed-rank tests.

Drosophila T4 recordings

In this paper, the data from *Drosophila* direction-selective neuron T4 was previously published as follows: Figure 1[18]; Figures 3 and 4[27]; Figure 5[54]; Figure 6[30]; and Figure 7 and associated figures.[49] In all these datasets, GCaMP6f[34] was expressed in T4 neurons under a promotor that targeted T4 and T5 neurons, and the two neuron types were later separated by their responses to light and dark edges. 2P imaging was used to acquire traces of T4 neuronal activity in response to visual stimuli displayed on a panoramic screen around the fly.[118] Figure 7 contains previously unpublished data taken with the same protocols as other data in the figure[49]; in order to stringently select for T4 signals, all data are from regions of interest in which a centered light-bar response was 3-fold larger or more than the dark-bar responses.